ISTANBUL TECHNICAL UNIVERSITY ★ GRADUATE SCHOOL OF SCIENCE
ENGINEERING AND TECHNOLOGY

AN INTEGRAL EQUATION METHOD WITH HERMITE SURFACES FOR PARTICLE SEDIMENTATION PROBLEMS

M.Sc. THESIS

Reşit Kayhan ATA

Department of Aeronautics and Astronautics Engineering

Aeronautics and Astronautics Engineering Programme

JANUARY 2014

ISTANBUL TECHNICAL UNIVERSITY ★ GRADUATE SCHOOL OF SCIENCE
ENGINEERING AND TECHNOLOGY

AN INTEGRAL EQUATION METHOD WITH HERMITE SURFACES FOR PARTICLE SEDIMENTATION PROBLEMS

M.Sc. THESIS

Reşit Kayhan ATA
(511111152)

Department of Aeronautics and Astronautics Engineering

Aeronautics and Astronautics Engineering Programme

Thesis Advisor: Assoc. Prof. Dr. Mehmet ŞAHİN

JANUARY 2014

İSTANBUL TEKNİK ÜNİVERSİTESİ ★ FEN BİLİMLERİ ENSTİTÜSÜ

PARÇACIK SEDİMANTASYON PROBLEMLERİ İÇİN HERMITE YÜZEYLERİ İLE İNTEGRAL DENKLEM YÖNTEMİ

YÜKSEK LİSANS TEZİ

Reşit Kayhan ATA
(511111152)

Uçak ve Uzay Mühendisliği Anabilim Dalı

Uçak ve Uzay Mühendisliği Programı

Tez Danışmanı: Assoc. Prof. Dr. Mehmet ŞAHİN

OCAK 2014

Reşit Kayhan ATA, an M.Sc. student of ITU Graduate School of Science Engineering and Technology 511111152 successfully defended the thesis entitled **"AN INTEGRAL EQUATION METHOD WITH HERMITE SURFACES FOR PARTICLE SEDIMENTATION PROBLEMS"**, which he prepared after fulfilling the requirements specified in the associated legislations, before the jury whose signatures are below.

Thesis Advisor :	**Assoc. Prof. Dr. Mehmet ŞAHİN** Istanbul Technical University	....
Jury Members :	**Prof. Dr. Can Fuat DELALE** Işık University	....
	Assist. Prof. Dr. Bayram ÇELİK Istanbul Technical University	....

Date of Submission : **16 December 2013**
Date of Defense : **21 January 2014**

FOREWORD

This thesis examine the numerical solution for the three dimensional Stokes flow to understand the motion of sedimenting particles. I really thank to my advisor Assoc. Prof. Dr. Mehmet ŞAHİN for his help in this work and my family for their support in my whole life.

January 2014

Reşit Kayhan ATA
Research Assisant

TABLE OF CONTENTS

Page

ABBREVIATIONS

NP	**:** Number of Points
NE	**:** Number of Elements
NB	**:** Number of Bodies
MWSELR	**:** Mean Weighted by Sine and Edge Length Reciprocal
MWE	**:** Mean Weighted Equally
MWA	**:** Mean Weighted by Angle
MWELR	**:** Mean Weighted by Edge Length Reciprocal
MWAAT	**:** Mean Weighted by Areas of Adjacent Triangles
DVBIE	**:** Direct Velocity Boundary Integral Equation
DTBIE	**:** Direct Traction Boundary Integral Equation
IVBIE	**:** Indirect Velocity Boundary Integral Equation

LIST OF TABLES

LIST OF FIGURES

Page

LIST OF SYMBOLS

ρ	:	Density
t	:	Time
$\mathbf{u}$	:	Linear velocity
P	:	Pressure
μ	:	Viscosity
$\mathbf{g}$	:	Gravitational force
∇	:	Nabla operator
∇^2	:	Laplace operator
Re	:	Reynolds number
Fr	:	Froude number
δ	:	Dirac delta function
$\mathbf{x}_0$	:	Position vector of source point
$\mathbf{x}$	:	Position vector of field point
σ	:	Stress field
ε	:	Small distance parameter
$\boldsymbol{\omega}$	:	Angular velocity
$\mathbf{S}$	:	Stokeslet
$\mathbf{T}$	:	Stress tensor
$\mathbf{t}$	:	Traction vector
N	:	Shape function
J	:	Jacobian matrix
$\mathbf{n}$	:	Normal vector
λ	:	Strength of singularity in Duffy transformation
β	:	Arbitrary constant in Duffy transformation
γ	:	Arbitrary constant in Duffy transformation
D	:	Drag
R	:	Radius
ψ	:	Stream function
I	:	Moment of inertia
$\mathbf{F}$	:	Force
$\mathbf{M}$	:	Torque
m	:	Mass
G	:	Fundamental solution of Laplace equation
H	:	Fundamental solution of Biharmonic equation
ε_{rr}	:	Viscous stress tensor component in rr direction
$\varepsilon_{r\theta}$	:	Viscous stress tensor component in $r\theta$ direction

AN INTEGRAL EQUATION METHOD WITH HERMITE SURFACES FOR PARTICLE SEDIMENTATION PROBLEMS

SUMMARY

An integral equation method has been developed to solve the three-dimensional Stokes flow using a quadrilateral Hermite based function approach to the boundary integral equation method. Then the numerical solutions are obtained by utilizing the boundary collocation method as well as the continuous distribution of Stokeslets, which are the fundamental solutions of the steady Stokes equations. The solution domain is divided into unstructured quadrilateral finite elements and the equations for the velocity and the pressure are solved on each element on the boundary surface. As an advantage of the boundary integral equation method, there is no need to construct a volume mesh, therefore the solution of full three dimensional problem is reduces to a two dimensional problem. In order to get smooth distribution in the numerical solution, the quadrilateral surface elements are represented by continuous parametric surfaces based on the bi-cubic Hermite functions that allows the continuous variation of the surface normal vectors between neighbouring elements. The problem of unique normal vectors at the vertices are solved by using the Mean Weighted by Sine and Edge Length Reciprocal (MWSELR) method after a comparison of vertex normal computation algorithms in the literature. The kernels of the integral equations have singularities. In order to calculate such singular integrals the $tanh - sinh$ quadrature method is used. Non-singular integrals are evaluated using the Gauss-Legendre quadrature rule. The numerical algorithm is initially validated for the three-dimensional unbounded Stokes flow around a sphere and the results are compared with the analytical solution. Then the algorithm is applied to the sedimentation of spherical particles. For the time discretization, first order backward differencing is employed.

PARÇACIK SEDİMANTASYON PROBLEMLERİ İÇİN HERMITE YÜZEYLERİ İLE İNTEGRAL DENKLEM YÖNTEMİ

ÖZET

Stokes akışı, bir başka ismiyle düşük Reynolds sayılı akışlar, atalet kuvvetlerinin viskoz kuvvetlere oranla çok küçük ve ihmal edilebilir olduğu akışlardır. Bu tip akışlarda Reynolds sayısı (atalet kuvvetlerinin viskoz kuvvetlere oranını gösteren boyutsuz sayı) birden çok küçüktür. Stokes akışının literatürdeki çeşitli uygulamalarından bazıları kılcal damarlardaki kan akışı, damlacık parçalanması, çok parçacıklı akışlar, sedimantasyon ve bakteri, kan hücresi, mikro robotlar gibi mikro yüzücüler etrafındaki akışlardır.

Son yıllarda sınır integral yöntemleri, Stokes akışı gibi küçük Reynolds sayılı akışların davranışlarını anlamak için çok güçlü birer teknik haline gelmişlerdir. Bu yöntemin üç boyutlu Stokes akışına uygulanması ilk olarak Youngren ve Acrivos (1975) tarafından, tek bir katı parçacık etrafındaki akışın, parçacık yüzeyindeki Stokeslet dağılımı ile yapılmıştır. Ardından yöntem farklı birçok akış problemi için uyarlanmıştır. Bunlardan bazıları, şekil değiştiren damla ve kabarcıklar etrafındaki akış, katı cisimlerin süspansiyon akışları, gözenekli ortamlardaki mikroskobik akışlar, kırmızı kan hücrelerinin deformasyonu ve mikroskobik organizmaların akışkan içindeki hareketidir.

Sınır integral yöntemlerinin başlıca avantajlarından birisi tamamen üç boyutlu olan bir akış problemini, yüzey elemanlarının kaynak dağılımlarını kullanarak iki boyutlu bir probleme dönüştürmesidir. Böylece hacim için çözüm ağı oluşturmaya gerek kalmaz. Ayrıca dış akış problemleri için uzak sınır koşulları tamamen sağlanmış olur. Ancak bu yöntemlerin bazı dezavantajları da mevcuttur. Bunlardan ilki algoritma sonucu büyük yoğun matrislerden oluşan cebirsel denklem sistemi oluşur ve bu sistemi paralel makinalarla çözülmesi oldukça zordur. İkinci olarak, integral formülasyonda tekillikler oluşmaktadır. Bu tekillikler özel uygulamalar gerektirmektedir.

Mevcut çalışmada üç boyutlu Stokes akışı için sürekli parametrik yüzeyler kullanılarak bir sınır integral eleman yöntemi geliştirilmiştir. İlk olarak, akışkan hareketinin temel denklemleri olan Navier-Stokes denklemleri sıkıştırılamaz ve Newtonian akışkan kabulü yapılarak yeni bir forma getirilmiştir. Ardından bu denklem sistemi boyutsuz parametreler kullanılarak boyutsuzlaştırılmıştır. Boyutsuz denklem Reynolds sayısının birden çok küçük olması durumu için tekrar düzenlenerek Stokes akışı için süreklilik ve momentum denklemleri çıkartılmıştır.

Stokes akışı için momentum denklemi sabit katsayılı lineer bir diferansiyel denklem olduğundan temel çözümü mevcuttur. Hız ve gerilim vektörleri için bu temel

çözümler elde edildikten sonra Stokes denklemleri sınır integral denklemine dönüştürülür. Bu çalışmada, sınır koşulları olarak yüzeylerdeki hızlar verildiğinden elde edilen denklemler birinci tip Fredholm denklemleridir. Bu tip denklemler "ill-conditioned" denklemler olmasına rağmen integral denklem yöntemlerinde yaygın olarak kullanılmaktadır. Bunun nedeni integral içindeki terimlerin bazı özel durumlarında bu "ill-conditioned" durumunun düzeltilebilir olmasıdır.

Elde edilen formülasyonun sayısal olarak çözülebilmesi için çözüm alanı dörtgen sonlu elemanlara ayrıklaştırılmış ve denklemler her bir eleman için çözülmüştür. Çözümün düzgün bir dağılım göstermesi için bu elemanların kesişim yerlerinde sürekliliğin sağlanması gerekmektedir. Bu amaçla her eleman üzerinde sürekli yüzeylerin tanımlanması gerekmektedir. İki boyutlu elemanlara uygulanabilecek sürekli yüzeylerden bir tanesi bi-kübik Hermite yüzeylerdir. Elemanlar üzerinde Hermite yüzeyleri tanımlayabilmek için nokta koordinatlarının ve eğimlerin bilinmesi gerekmektedir. Noktaların koordinatları çözüm ağı bilgisinden gelmektedir, bu noktalardaki eğimler ise noktalardaki normal vektörü kullanılarak hesaplanmaktadır. Ancak bu hesaplamanın yapılabilmesi için çözüm ağındaki her bir nokta için tek bir normal vektör olması gerekmektedir. Bunu sağlamak üzere, literatürde normal vektörü hesaplama algoritmaları karşılaştırılmış ve en uygun yöntem seçilmiştir. Bu yöntem, eleman kenar uzunlukları ve aralarındaki açıları kullanan bir algoritmadır

Denklemlerdeki integrallerin de sayısal olarak hesaplanması gerekmektedir. Ancak elde edilen integral denklemler bazı noktalarda tekillik göstermektedir. Tekil olmayan integraller hesaplanırken klasik Gauss-Legendre yöntemi kullanılmıştır. Gauss-Legendre yönteminde dörtgen üzerinde belirli sayıda hesaplama noktaları ve bu noktalar için ağırlıklar belirlenir ardından fonksiyonun eleman üzerindeki dağılımı hesaplanır. Bu çalışmada 4 noktalı Gauss-Legendre yöntemi ($n = 4$) kullanılmıştır, böylece elemanlar üzerinde toplam 16 hesaplama noktası bulunmaktadır.

Tekil fonksiyonların integrasyonu analitik olarak veya özel sayısal yöntemler kullanılarak hesaplanabilir. Sayısal integrasyon yöntemleri genellikle değişken dönüşümü yöntemlerine dayanır. Böylece elemanlar üzerindeki hesaplama noktaları tekilliğin olduğu nokta civarına kaydırılır. Yapılan literatür araştırmasının ardından tekil integraller için *tanh-sinh* yöntemi kullanılmıştır. Bu yöntem $[-1,1]$ olan integral aralığını $[-\infty,+\infty]$ olarak değiştirir. Böylece hesaplama noktaları tekilliğin olduğu noktaya kaydırılarak tekillik giderilir. Eleman üzerinde kaç hesaplama noktası olacağı bu yöntemin seviyesine (m) bağlıdır. Bu çalışmada problemin hassasiyetine göre 2-4 arası seviyeler kullanılmıştır. $m = 2$ için eleman üzerinde 21×21, $m = 4$ için 87×87 nokta bulunmaktadır.

Elde ettiğimiz sayısal algoritma ilk olarak sabit duran tek küre etrafındaki akış için uygulanmıştır. Bu problem için faklı eleman sayılarına sahip üç farklı çözüm ağı denenmiştir. Bulunan sayısal sonuçlar analitik çözüm ile karşılaştırılmış ve eleman sayısının artmasıyla çözümün analitik çözüme oldukça yaklaştığı görülmüştür.

İkinci olarak algoritma yer çekimi etkisinde serbest düşen küreler için denenmiştir. Öncelikle tek başına düşen küre için çözüm yapılmıştır. Bu çözümün doğruluğunu karşılaştırabilmek için ilk problemde bulunan sürükleme kuvveti bu problemde ağırlık olarak verilmiştir. Böylece kürenin belirli bir zamandan sonra ilk problemdeki sabit hıza ulaşması beklenmiştir ve sonuçlar beklenildiği gibi çıkmıştır. Ardından yer çekimi etkisindeki iki küre problemi ele alınmıştır. Literatürde bulunan bir test problemi denenmiş ve sonuçlar karşılaştırılmıştır. Karşılaştırma sonucu çözümlerin yakın olduğu görülmüştür. Bunun üzerine iki küre problemi farklı bir konfigürasyon için uygulanmıştır.

Son olarak üç küre problemi incelenmiştir. Başlangıçta hareketsiz ve yan yana duran üç küre serbest düşmeye bırakılmıştır. Çözümün ardından ortadaki kürenin diğer ikisine göre daha hızlı düştüğü ve diğerlerinin birbirine yaklaştığı görülmüştür. Literatürdeki önceki çalışmalar da bu şekilde sonuçlar vermektedir. Ancak zaman ilerledikçe yanlarda duran kürelerin birbirine iyice yaklaştığı ve sonunda birbirinin içine geçtiği görülmüştür. Bunun nedeni viskoz akışlarda birbirine çok yaklaşan cisimlerin arasında oluşan yağlama kuvvetleridir. Bu kuvvetlerin sayısal olarak yakalanabilmesi için cisimler birbirine yaklaştığında çözünürlüğün artırılması ve zaman adımının düşürülmesi gerektiği görülmüştür.

Bu çalışmanın amacı bi-kübik Hermite polinomları ve tanh-sinh yöntemini beraber kullanarak, integral denklem yöntemine dayalı stabil bir Stokes çözücüsü geliştirmektir. Sayısal algoritma için, yüzeyler üzerinde düzensiz dörtgen elemanlar kullanılmıştır ve bilinmeyen fonksiyon değerleri elemanların köşe noktalarına dağıtılmıştır. Zamanda birinci dereceden geri yönde farklar yöntemi ile ayrıklaştırma yapılmıştır. Tüm hesaplamalar Intel(R) Core(TM) i7-2770 340 Ghz işlemcili ve 16 GB hafızaya sahip bir masaüstü bilgisayarda yapılmıştır.

1. INTRODUCTION

Stokes flow, or sometimes called creeping flow or low Reynolds number flow, is defined to be a very viscous flow where inertia forces are negligible relative to viscous forces. It is named after Sir George Gabriel Stokes. The Stokes flow has a wide range of applications such as blood flow in capillaries, droplet break-up, multi particles flows or sedimentation, flows around micro swimmers like bacteria, blood cell, micro robotics, etc.

Over the past decades, the boundary integral methods have emerged to be a very powerful technique for studying the flow behaviour at vanishingly small Reynolds numbers, i.e. under the Stokes flow conditions. The application of the present method to the three-dimensional Stokes flow was first formulated by Youngren and Acrivos [1] for an unbounded fluid past a single solid particle as a distribution of Stokeslets over the particle surface. Then the method was quickly adopted for several other flow problems at very low Reynolds numbers including the flow past deformable droplets and bubbles [2], the flows of suspensions of rigid particles [3], the microscopic flow in porous media [4], the deformation of red blood cells [5], the swimming of microscopic organisms [6], etc.

The main advantages of the boundary integral equation method is that it reduces the solution of full three-dimensional fluid flow problem into a two-dimensional problem of determining source distributions on the bounding surfaces, which does not require the construction of volume mesh. In addition, the far-field boundary conditions are satisfied exactly for exterior fluid flow problems. However, the numerical approach has also several disadvantages. The first one is that the numerical algorithm does lead to a dense system of algebraic equations and it is very difficult to implement efficiently on highly parallel machines. The second one is that the integral equation formulation leads to singular integral which requires special treatment.

The integration of the singular functions can be calculated either analytically or by using special numerical techniques. The numerical integration techniques are mostly based on the variable mappings which cluster quadrature points close to the

position of the singularity. Muldowney and Higdon [7] showed that the transformed quadrature methods for singular and nearly singular integrals can be constructed for the requirements of the spectral element. Chan et al. [8] proposed an adaptive sub-domain integration scheme that dramatically improved the integration accuracy and provided convergent solutions for problems of very small gaps. Duffy [9] suggested a transformation of integration for pyramids and cubes at singular vertices, Mousavi and Sukumar [10] developed this method for two dimensions using a transformation a triangular surface having a singular vertex into an integration over a unit square. These transformations cancels the singularity. However, the latter approach can be applied to only planar surfaces and is accurate only for sufficiently regular triangles. In addition, there is another type of approach which replaces singular kernel by a regularized kernel [11]. An another approach is to employ the $tanh - sinh$ quadrature rule proposed by Takahasi and Mori [12]. This approach uses change of variables to transform an integral on the interval [-1,1] to an integral between $[-\infty,\infty]$. After the transformation, the integrand decays with a double exponential rate. Although $tanh - sinh$ quadrature is less efficient than Gaussian quadrature for smooth integrands, in contrast to Gaussian quadrature, it tends to work equally well with integrands having singularities or infinite derivatives at one or both endpoints of the integration interval.
Although the singular kernel could be evaluated using the transformed quadrature methods, the discontinuities in the normal vector around the collocation/singularity point may cause irregularities in the numerical solution. One possible approach to remedy the numerical solution is to employ more smooth variation of boundary surface. A bi-cubic Hermite polynomial which yields smoothly blended surface elements can be employed over unstructured quadrilateral elements. The Hermite polynomial interpolation requires the function value and its derivatives at the vertices. Although the coordinate of vertices are known, the tangent values at vertices has to be computed. The tangent values can be calculated from the unique normal vector at vertices.

The purpose of the present work is to combine the bi-cubic Hermite polynomial with the $tanh - sinh$ quadrature rule in order to develop a sufficiently robust Stokes solver based on the integral equation formulation. The numerical algorithm uses unstructured quadrilateral elements over the domain boundaries and the unknown function values are distributed over the vertices of quadrilateral elements. The singular integrations are evaluated numerically using the $tanh-sinh$ quadrature rule meanwhile non-singular integrals are evaluated using Gauss-Legendre quadrature rule. The numerical algorithm is initially validated for the three-dimensional unbounded Stokes flow around a sphere. Then the algorithm is applied to the sedimentation of spherical particles.

2. MATHEMATICAL FORMULATION

Since the inertia terms in the momentum equation of the Stokes flow are negligible, which means the Reynolds number is vanishingly small ($Re << 1$), therefore the Stokes flow equations can be derived under these assumptions. These basic assumptions are developed by Sir George Gabriel Stokes in 1851. The details of the derivation of the Stokes equations starting from the Navier-Stokes equations are given in the next section.

2.1 Governing Equations of the Stokes Flow

Fluid motion can be described mathematically using the Navier-Stokes equations in terms of velocity and pressure

$$\frac{\partial \rho}{\partial t} + \nabla \cdot (\rho \mathbf{u}) = 0 \quad \textbf{(2.1)}$$

$$\frac{\partial (\rho \mathbf{u})}{\partial t} + \mathbf{u} \cdot \nabla (\rho \mathbf{u}) = -\nabla P + \mu \nabla^2 \mathbf{u} + \rho \mathbf{g} \quad \textbf{(2.2)}$$

The first equation is the continuity and the second one is the momentum equation of the fluid flow. Here, $\mathbf{u}$ is the fluid velocity vector, ρ is the density of the fluid, μ the viscosity of the fluid, P is the pressure and $\mathbf{g}$ is the body force.

For incompressible and Newtonian fluids where the density and the viscosity are constant, these equations can be reduced to the following form

$$\nabla \cdot \mathbf{u} = 0 \quad \textbf{(2.3)}$$

$$\rho \left(\frac{\partial \mathbf{u}}{\partial t} + \mathbf{u} \cdot \nabla \mathbf{u} \right) = -\nabla P + \mu \nabla^2 \mathbf{u} + \rho \mathbf{g} \quad \textbf{(2.4)}$$

In fluid dynamics, equations generally are written in dimensionless form. In order to get these non-dimensional equations, all variables are replaced by dimensionless parameters using the characteristic variables which can be seen in the Table 2.1. After substituting these variables into the equation (2.4) the non-dimensional momentum equation becomes

$$\rho \frac{U^2}{L} \left(\frac{\partial \mathbf{u}^*}{\partial t^*} + \mathbf{u}^* \cdot \nabla \mathbf{u}^* \right) = -\frac{\mu U}{L^2} \nabla P^* + \frac{\mu U}{L^2} \nabla^2 \mathbf{u}^* + \rho g \mathbf{g}^* \quad \textbf{(2.5)}$$

Table 2.1: Variables for non-dimensionalization.

Scale	Variable	Characteristic variable	non-dimensional variable
Velocity	$\mathbf{u}$	U	$\mathbf{u}^* = \mathbf{u}/U$
Length	$\mathbf{x}$	L	$\mathbf{x}^* = \mathbf{x}/L$
Time	t	L/U	$t^* = tU/L$
Pressure	P	$\mu U/L$	$P^* = PL/\mu U$
Gravity	$\mathbf{g}$	g	$\mathbf{g}^* = \mathbf{g}/g$

Multiplying whole equation by $L/\rho U^2$ and arranging the coefficients, the following equation can be derived

$$\frac{\partial \mathbf{u}^*}{\partial t^*} + \mathbf{u}^* \cdot \nabla \mathbf{u}^* = -\frac{1}{Re}\nabla P^* + \frac{1}{Re}\nabla^2 \mathbf{u}^* + \frac{1}{Fr}\mathbf{g}^* \tag{2.6}$$

Here, Re and Fr are the Reynolds and the Froude numbers, respectively, and they are dimensionless parameters. The Reynolds number is the ratio of inertial forces to viscous forces, $Re = \rho UL/\mu$. The Froude number is the ratio of inertial forces to gravitational forces, $Fr = U^2/gL$. Then the equation (2.6) can be rewritten in the following form

$$Re\left(\frac{\partial \mathbf{u}^*}{\partial t^*} + \mathbf{u}^* \cdot \nabla \mathbf{u}^*\right) = -\nabla P^* + \nabla^2 \mathbf{u}^* + \frac{Re}{Fr}\mathbf{g}^* \tag{2.7}$$

Therefore, incompressible fluid flow problems where viscous forces are dominant over inertial forces ($Re << 1$) can be described by the Stokes equations

$$\nabla \cdot \mathbf{u} = 0 \tag{2.8}$$

$$-\nabla P + \mu \nabla^2 \mathbf{u} + \rho \mathbf{g} = 0 \tag{2.9}$$

Since the gravitational force field is conservative, it can be combined with the pressure, therefore the equation (2.9) reduces to

$$-\nabla P + \mu \nabla^2 \mathbf{u} = 0 \tag{2.10}$$

The Stokes equations are linear and have constant coefficients. Hence, it is easier to solve analytically and numerically compared to the Navier-Stokes equations.

2.2 The Fundamental Solutions of the Stokes Equations

The Stokes equations are linear partial differential equation with constant coefficients and for any such differential equation there is a fundamental solution [13]. The potential equation is given by

$$\nabla^2 u = 0 \tag{2.11}$$

Now let $\mathbf{x}_0$ be a source point, and $\mathbf{x}$ be a field point in the domain. The density of $\mathbf{x}_0$ at $\mathbf{x}$ is expressed by the relation

$$\delta(\mathbf{x}_0 - \mathbf{x}) \tag{2.12}$$

where δ is the Dirac delta function. This expression satisfies the equation (2.11) and it is called the *fundamental solution* of the potential equation (2.11) [14].

There are several fundamental solutions to the Stokes flow depending on the dimension and the topology of the problem. In this study, the flow is three dimensional, infinite and unbounded. Hence in this work the free-space Green's function for fundamental solution will be used [15]. The Stokes equations can be written as

$$\nabla P - \mu \nabla^2 \mathbf{u} \;=\; \mathbf{f}\delta(\mathbf{x} - \mathbf{x}_0) \tag{2.13}$$

Here, $\mathbf{f}$ is a point force and it is constant. δ is the three-dimensional Dirac delta function. $\mathbf{x}_0$ and $\mathbf{x}$ are the source point and field point, respectively. The derivation of the fundamental solution or the free-space Green's function to the Stokes equations can be found in [15], [16] and [17]. In order to get the fundamental solution, the fundamental solutions of the Laplace and Biharmonic equations are used because they satisfy the following equations

$$\nabla^2 G(r) \;=\; \delta(r) \tag{2.14}$$

$$\nabla^4 H(r) \;=\; \delta(r) \tag{2.15}$$

First, taking the divergence of the equation (2.13)

$$\nabla \cdot (\nabla P - \mu \nabla^2 \mathbf{u}) \;=\; \nabla \cdot [\mathbf{f}\delta(\mathbf{x} - \mathbf{x}_0))] \tag{2.16}$$

Remember that the divergence and Laplace operators are commutative, then applying the product rule for the right hand side gives

$$\nabla^2 P - \mu \nabla^2 (\nabla \cdot \mathbf{u}) \;=\; \delta \nabla \cdot \mathbf{f} + \mathbf{f} \cdot \nabla \delta(\mathbf{x} - \mathbf{x}_0) \tag{2.17}$$

From the continuity $\nabla \cdot \mathbf{u} = 0$. Since $\mathbf{f}$ is constant, then $\nabla \cdot \mathbf{f} = 0$. Therefore,

$$\nabla^2 P \;=\; \mathbf{f} \cdot \nabla \delta(\mathbf{x} - \mathbf{x}_0) \tag{2.18}$$

Using the equation (2.14)

$$P = \mathbf{f} \cdot \nabla G \tag{2.19}$$

Insert this expression into the equation (2.13). Recall that $\nabla^2 G = \delta(\mathbf{x} - \mathbf{x}_0)$

$$\nabla(\mathbf{f} \cdot \nabla G) - \mu \nabla^2 \mathbf{u} = \mathbf{f} \delta(\mathbf{x} - \mathbf{x}_0) \tag{2.20}$$

$$\mu \nabla^2 \mathbf{u} = \mathbf{f}(\nabla \nabla G) - \mathbf{f} \delta(\mathbf{x} - \mathbf{x}_0) \tag{2.21}$$

$$\mu \nabla^2 \mathbf{u} = \mathbf{f}[\nabla \nabla - \mathbf{I} \nabla^2] G \tag{2.22}$$

In here, $\mathbf{I}$ is the identity matrix. Using $\nabla^2 G = \nabla^4 H$

$$\mu \nabla^2 \mathbf{u} = \mathbf{f}[\nabla^2 \nabla^2 - \mathbf{I} \nabla^4] H \tag{2.23}$$

$$\mu \mathbf{u} = \mathbf{f}[\nabla \nabla - \mathbf{I} \nabla^2] H \tag{2.24}$$

The fundamental solution of the Laplacian is the following

$$G = -\frac{1}{4\pi r} \tag{2.25}$$

Hence

$$\nabla^2 H = -\frac{1}{4\pi r} \tag{2.26}$$

In order to find such H, we need to write the Laplace equation in the spherical coordinates

$$\nabla^2 H = \frac{1}{r^2} \frac{\partial}{\partial r} \left(r^2 \frac{\partial H}{\partial r} \right) + \frac{1}{r^2 \sin \theta} \left(\sin \theta \frac{\partial H}{\partial \theta} \right) + \frac{1}{r^2 \sin^2 \theta} \frac{\partial^2 H}{\partial \phi^2} \tag{2.27}$$

Since we only consider the radial changes, the second and third terms on the right hand side can be neglected leading the following equation

$$\nabla^2 H = \frac{1}{r^2} \frac{\partial}{\partial r} \left(r^2 \frac{\partial H}{\partial r} \right) \tag{2.28}$$

Integrating this expression twice for $H(0) = 0$

$$r^2 \frac{\partial H}{\partial r} = -\frac{r^2}{8\pi} \tag{2.29}$$

$$H(r) = -\frac{r}{8\pi} \tag{2.30}$$

Substituting this expression into equation (2.24) gives

$$\mathbf{u}(\mathbf{x}) = -\frac{\mathbf{f}}{8\pi\mu} [\nabla \nabla - \mathbf{I} \nabla^2] r \tag{2.31}$$

This expression can be written as

$$u_i(\mathbf{x}) \;=\; -\frac{f_j}{8\pi\mu}\left(\frac{\delta_{ij}}{r}+\frac{\hat{x}_i\hat{x}_j}{r^3}\right) \qquad \textbf{(2.32)}$$

In here $r = |\hat{\mathbf{x}}| = |\mathbf{x}-\mathbf{x}_0|$ and the second term on the right hand side is called the fundamental solution to the Stokes flow or *Stokeslet*. It may also be called *Oseen-Burger tensor*.

$$S_{ij}(\hat{\mathbf{x}}) \;=\; \frac{\delta_{ij}}{r}+\frac{\hat{x}_i\hat{x}_j}{r^3} \qquad \textbf{(2.33)}$$

Hence the velocity field of the Stokes flow is written

$$u_i(\mathbf{x}) \;=\; -\frac{1}{8\pi\mu}S_{ij}(\hat{\mathbf{x}})f_j \qquad \textbf{(2.34)}$$

The pressure and stress field for this flow can be written as

$$P(\mathbf{x}) \;=\; \frac{1}{8\pi}p_j(\hat{\mathbf{x}})f_j \qquad \textbf{(2.35)}$$

$$\sigma_{ik}(\mathbf{x}) \;=\; \frac{1}{8\pi}T_{ijk}(\hat{\mathbf{x}})f_j \qquad \textbf{(2.36)}$$

where $\mathbf{p}$ and $\mathbf{T}$ are associated with the pressure vector and stress tensor. Therefore, the equation (2.34) satisfies both the continuity and the momentum equation. Then taking the divergence of the equation (2.34)

$$\nabla\cdot\mathbf{u} \;=\; \nabla\cdot\left(-\frac{1}{8\pi\mu}\mathbf{S}(\hat{\mathbf{x}})\mathbf{f}\right) \qquad \textbf{(2.37)}$$

Using the continuity equation

$$\nabla\cdot\mathbf{S} \;=\; 0 \qquad \textbf{(2.38)}$$

or

$$\frac{\partial S_{ij}}{\partial x_i}(\hat{\mathbf{x}}) \;=\; 0 \qquad \textbf{(2.39)}$$

Inserting the equations (2.34) and (2.35) into the momentum equation (2.13)

$$\frac{1}{8\pi}\nabla\cdot[p(\hat{\mathbf{x}})\mathbf{f}]-\mu\nabla^2\cdot\left[\frac{1}{8\pi\mu}\mathbf{S}(\hat{\mathbf{x}})\mathbf{f}\right] \;=\; \mathbf{f}\delta(\mathbf{x}-\mathbf{x}_0) \qquad \textbf{(2.40)}$$

After some mathematical operations

$$\nabla p(\hat{\mathbf{x}})-\nabla^2\mathbf{S}(\hat{\mathbf{x}}) \;=\; 8\pi\delta(\mathbf{x}-\mathbf{x}_0) \qquad \textbf{(2.41)}$$

Taking the divergence of this equation using the equation (2.38)

$$\nabla^2 p(\hat{\mathbf{x}}) \quad = \quad 8\pi\nabla\delta(\mathbf{x}-\mathbf{x}_0) \tag{2.42}$$

Noting that $\nabla^2 G = \delta(\mathbf{x}-\mathbf{x}_0)$ and using the equation (2.25) the pressure tensor is derived as follows

$$p_i(\hat{\mathbf{x}}) \quad = \quad 2\frac{\hat{x}_i}{r^3} \tag{2.43}$$

The equation for stress is given by

$$\sigma_{ik}(\mathbf{x}) \quad = \quad -\delta_{ik}P(\mathbf{x})+\mu\left(\frac{\partial u_i}{\partial x_k}+\frac{\partial u_k}{\partial x_i}\right) \tag{2.44}$$

Substituting the relations (2.33) to (2.36) and (2.43) into the equation (2.44) the following stress tensor $\mathbf{T}$ is derived

$$T_{ijk}(\hat{\mathbf{x}}) \quad = \quad -6\frac{\hat{x}_i\hat{x}_j\hat{x}_k}{r^5} \tag{2.45}$$

2.3 The Boundary Integral Formulation

The momentum equation of the Stokes flow (2.10) is a linear differential equation with constant coefficients, therefore, it can be written in integral form. For boundary value problems, using the integral equations provides several advantages. First, the integral equation operator is usually bounded and generally continuous. Second, they involve same boundary conditions at the infinity, therefore the solutions of the integral equations satisfy these boundary conditions automatically [18]. The boundary integral methods use the velocities and tractions on the bounding surface to compute the velocities at any point in the flow field. Therefore, they reduce the complexity of a three-dimensional problem into a two-dimensional surface problem. [19].

In order to derive the boundary integral formulation it is convenient to start from Lorentz reciprocal theorem for an incompressible Newtonian fluid flow

$$\nabla\cdot(\mathbf{u}\cdot\sigma')-\nabla\cdot(\mathbf{u}'\cdot\sigma) \tag{2.46}$$

The derivation of the theorem can be found in [19], [20], [21]. Note that σ and σ' are the corresponding stress tensors of $\mathbf{u}$ and $\mathbf{u}'$, respectively, for a regular (non-singular) flow. Using the equations (2.34) and (2.36) for $\mathbf{u}'$ and σ' and substituting them into the equation (2.46)

$$\frac{\partial}{\partial x_k}[S_{ij}(\hat{\mathbf{x}})\sigma_{ik}(\mathbf{x})-\mu u_i(\mathbf{x})T_{ijk}(\hat{\mathbf{x}})] \quad = \quad 0 \tag{2.47}$$

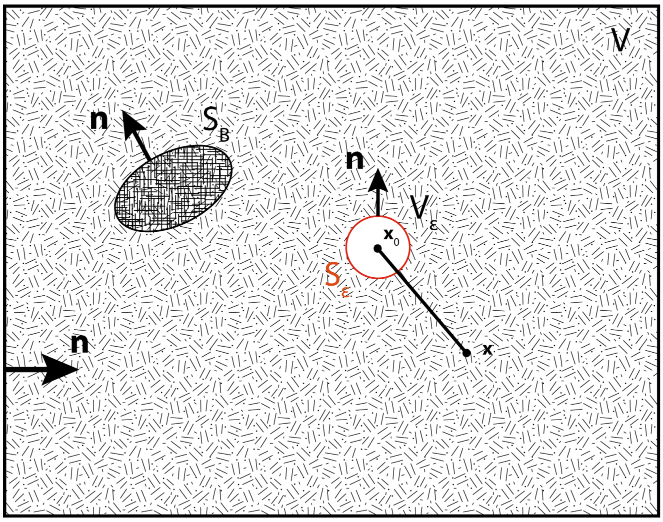

Figure 2.1: Control volume in fluid domain.

Integrating this equation over the control volume V and applying the divergence theorem to convert the volume integral into the surface integral on the surface S_B bounding the volume V

$$\oiint_{S_B} [S_{ij}(\hat{\mathbf{x}})\sigma_{ik}(\mathbf{x}) - \mu u_i(\mathbf{x}) T_{ijk}(\hat{\mathbf{x}})] n_k(\mathbf{x}) dS(\mathbf{x}) = 0 \tag{2.48}$$

Here $\mathbf{n}$ is the surface normal vector directed to the control volume. Now consider a small control volume V_ε with radius ε inside V bounded by the surface S_ε placed at $\mathbf{x}_0$ as seen in the Figure 2.1. The equation (2.48) is still valid for the new control volume with the surfaces S_B and S_ε. If the radius ε goes to zero, the tensors $\mathbf{S}$ and $\mathbf{T}$ become

$$S_{ij} = \frac{\delta_{ij}}{\varepsilon} + \frac{\hat{x}_i \hat{x}_j}{\varepsilon^3} \tag{2.49}$$

$$T_{ijk} = -6\frac{\hat{x}_i \hat{x}_j \hat{x}_k}{\varepsilon^5} \tag{2.50}$$

For the surface S_ε, the normal vector becomes $\mathbf{n} = \hat{\mathbf{x}}/\varepsilon$ and $dS = \varepsilon^2 d\Omega$ where Ω is the differential solid angle. Substituting these relations into the equation (2.48) for V_ε and subtracting from V gives

$$\begin{aligned} &\oiint_{S_B} [S_{ij}(\hat{\mathbf{x}})\sigma_{ik}(\mathbf{x}) - \mu u_i(\mathbf{x}) T_{ijk}(\hat{\mathbf{x}})] n_k(\mathbf{x}) dS(\mathbf{x}) = \\ &-\oiint_{S_\varepsilon} \left[\left(\frac{\delta_{ij}}{\varepsilon} + \frac{\hat{x}_i \hat{x}_j}{\varepsilon^3} \right) \sigma_{ik}(\mathbf{x}) + \mu u_i(\mathbf{x}) 6 \frac{\hat{x}_i \hat{x}_j \hat{x}_k}{\varepsilon^5} \right] \frac{\hat{x}_k}{\varepsilon} \varepsilon^2 d\Omega \end{aligned} \tag{2.51}$$

As ε goes to zero, $\hat{\mathbf{x}}$ and, therefore, σ go to zero as well. Therefore, the first term on the right hand side vanishes and after some mathematical operations

$$\begin{aligned}\oiint_{S_B} [S_{ij}(\hat{\mathbf{x}})\sigma_{ik}(\mathbf{x}) - \mu u_i(\mathbf{x})T_{ijk}(\hat{\mathbf{x}})]n_k(\mathbf{x})dS(\mathbf{x}) \\ = -6\pi u_i(\mathbf{x}_0)\frac{1}{\varepsilon^4}\oiint_{S_\varepsilon} \hat{x}_i\hat{x}_j dS(\mathbf{x})\end{aligned} \tag{2.52}$$

Applying the divergence theorem on the right hand side gives

$$\delta_{ij}\frac{4}{3}\pi\varepsilon^4 \tag{2.53}$$

Inserting this expression into the equation (2.52) the boundary integral formulation of the Stokes equations is derived

$$u_j(\mathbf{x}_0) = -\frac{1}{8\pi\mu}\oiint_{S_B} \left[S_{ij}(\hat{\mathbf{x}})t_i(\mathbf{x}) - \mu T_{ijk}(\hat{\mathbf{x}})u_i(\mathbf{x})n_k(\mathbf{x})\right] dS(\mathbf{x}) \tag{2.54}$$

In here, $\mathbf{t} = \sigma\mathbf{n}$ is the traction vector and the normal vector $\mathbf{n}$ points into the fluid domain. The first and second term on the right hand side are called *single-layer potential* and *double-layer potential*, respectively. The single-layer potential represents the flow due to a surface distribution of point forces while the double-layer potential represents the flow due to a surface distribution of the stress tensor $\mathbf{T}$. According to Odqvist [22], the Stokes flow can be represented by only the single-layer or double-layer potential and this approach is called *regularized* or *indirect boundary integral method*. For boundary value problems with velocity boundary conditions, the integral equation leads to the Fredholm integral equations of the first kind [15]

$$8\pi\mu u_j(\mathbf{x}_0) = \oiint_{S_B} t_i \left[\frac{\delta_{ij}}{r} + \frac{(x_i - x_{0_i})(x_j - x_{0_j})}{r^3}\right] dS(\mathbf{x}) \tag{2.55}$$

and the pressure field can be evaluated as follows

$$8\pi P(\mathbf{x}_0) = \oiint_{S_B} t_i \left[2\frac{x_i - x_{0_i}}{r^3}\right] dS(\mathbf{x}) \tag{2.56}$$

The first kind equations are ill-conditioned because the solution is very sensitive to small changes in the data function. But when the kernel of the equation (for the equations (2.55) and (2.56) the terms in the square brackets) is singular, then the ill-conditioning is manageable [23]. These single layer equations are easy to use for flows with ambient field which is given in a form that its stress field can be calculated easily. The single layer potential means that they are superposition of the hydrodynamic potentials of a point force. The potentials mentioned here are analogous to ones that are in the potential theory. The single layer potentials are continuous on the whole domain as long as the surface boundary is a Lyapunov surface. The Lyapunov surfaces have very good smoothness properties.

Using double layer potential instead of single layer, which corresponds to traction boundary condition, leads to the Fredholm integral equation of the second kind. The double layer potentials are caused by a layer of sources and doublets of point forces. The double layer potentials are discontinuous over the surface boundary. There is a jump in the velocity field across the exterior and the interior domain (see Figure 2.2) and they are not enough to represent the velocity field alone, hence the double layer equations need special treatment. This is the reason for the use of the Fredholm integral equations of the first kind even though they are ill-conditioned [1], [24], [25].

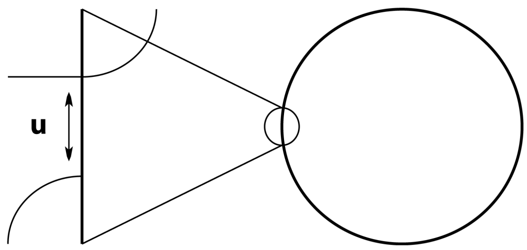

Figure 2.2: Jump in the double layer potential.

3. NUMERICAL FORMULATION

3.1 The Discretization of the Boundary Integral Equation

The solution domain is discretized into quadrilateral finite elements. The equations (2.55) and (2.56) become [26]

$$8\pi\mu u_j(\mathbf{x}) = \sum_{k=1}^{NE}\sum_{i=1}^{3}\oiint_{S_B} t_{ik}\left[\frac{\delta_{ij}}{r}+\frac{(x_i-x_{0_i})(x_j-x_{0_j})}{r^3}\right]dS(x) \tag{3.1}$$

$$8\pi P(\mathbf{x}) = \sum_{k=1}^{NE}\sum_{i=1}^{3}\oiint_{S_B} t_{ik}\left[2\frac{x_i-x_{0_i}}{r^3}\right]dS(x) \tag{3.2}$$

Here NE is the number of quadrilateral elements. $\mathbf{x}_0 = (x_{0_1}, x_{0_2}, x_{0_3})$ is the position vector of the source point. These equations are solved for each collocation point which correspond to verticies of the computational mesh. As an example the x-component of the velocity reads

$$\begin{aligned} 8\pi\mu u_1(\mathbf{x}) = &\sum_{k=1}^{NE}\oiint_{S_B} t_{1k}\left[\frac{1}{r}+\frac{(x_1-x_{0_1})^2}{r^3}\right]dS(x)\\ &+\sum_{k=1}^{NE}\oiint_{S_B} t_{2k}\left[\frac{(x_1-x_{0_1})(x_2-x_{0_2})}{r^3}\right]dS(x)\\ &+\sum_{k=1}^{NE}\oiint_{S_B} t_{3k}\left[\frac{(x_1-x_{0_1})(x_3-x_{0_3})}{r^3}\right]dS(x) \end{aligned} \tag{3.3}$$

Other components can be written in the same way

$$\begin{aligned} 8\pi\mu u_2(\mathbf{x}) = &\sum_{k=1}^{NE}\oiint_{S_B} t_{1k}\left[\frac{(x_2-x_{0_2})(x_1-x_{0_1})}{r^3}\right]dS(x)\\ &+\sum_{k=1}^{NE}\oiint_{S_B} t_{2k}\left[\frac{1}{r}+\frac{(x_2-x_{0_2})^2}{r^3}\right]dS(x)\\ &+\sum_{k=1}^{NE}\oiint_{S_B} t_{3k}\left[\frac{(x_2-x_{0_2})(x_3-x_{0_3})}{r^3}\right]dS(x) \end{aligned} \tag{3.4}$$

$$
\begin{aligned}
8\pi\mu u_3(\mathbf{x}) = &\sum_{k=1}^{NE} \oiint_{S_B} t_{1k} \left[\frac{(x_3 - x_{0_3})(x_1 - x_{0_1})}{r^3} \right] dS(x) \\
&+ \sum_{k=1}^{NE} \oiint_{S_B} t_{2k} \left[\frac{(x_3 - x_{0_3})(x_2 - x_{0_2})}{r^3} \right] dS(x) \\
&+ \sum_{k=1}^{NE} \oiint_{S_B} t_{3k} \left[\frac{1}{r} + \frac{(x_3 - x_{0_3})^2}{r^3} \right] dS(x)
\end{aligned}
\tag{3.5}
$$

And the pressure equation becomes

$$
\begin{aligned}
8\pi P(\mathbf{x}) = &\sum_{k=1}^{NE} \oiint_{S_B} t_{1k} \left[2\frac{x_1 - x_{0_1}}{r^3} \right] dS(x) \\
&+ \sum_{k=1}^{NE} \oiint_{S_B} t_{2k} \left[2\frac{x_2 - x_{0_2}}{r^3} \right] dS(x) \\
&+ \sum_{k=1}^{NE} \oiint_{S_B} t_{3k} \left[2\frac{x_3 - x_{0_3}}{r^3} \right] dS(x)
\end{aligned}
\tag{3.6}
$$

The integrals are to be computed numerically using the quadrature rules in Chapter 4.

3.2 Surface Smoothness

To apply the numerical formulation, the solution domain is divided into quadrilateral finite elements. Although these elements are continuous within the local elements, there are discontinuities between these elements. These discontinuities cause poor results in the numerical solution. In order to have smooth solution fields, these quadrilateral elements need to be represented by smooth parametric surfaces. There are several types of parametric surfaces that can be applied to two dimensional elements such as Bezier surfaces, B-spline surfaces and Hermite surfaces. For this study, Hermite surfaces are chosen to be employed due to their easy construction.

3.2.1 Quadrilateral Hermite surfaces

One way of creating surfaces is to move curves in a specified manner such as sweep, revolution, deformation or joining with other curves [27]. In this paper the smooth surfaces are created using the Hermite bi-cubic patch similar to the Hermite bi-cubic curves.

It was proven by the Euler beam theory that the best smoothed curves passing through a set of points are parametric polynomial cubic splines because they minimize the strain energy of the beam [28]. Ferguson represented a parametric cubic curve that has the following form [29]

$$r(u) = a_0 + a_1 u + a_2 u^2 + a_3 u^3 \tag{3.7}$$

In here $0 \leq u \leq 1$ and a_i are unknowns. This expression is known as Ferguson representation. Writing this equation and its derivatives at $u = 0$ and $u = 1$ as seen in the Figure 3.1

$$\begin{aligned} r(0) &= a_0 \\ r(1) &= a_0 + a_1 + a_2 + a_3 \\ r'(0) &= a_1 \\ r'(1) &= a_1 + 2a_2 + 3a_3 \end{aligned} \tag{3.8}$$

The a_i coefficients are expressed in terms of $r(u)$ and $r'(u)$

$$\begin{aligned} a_0 &= r(0) \\ a_1 &= r'(1) \\ a_2 &= 3[r(1) - r(0)] - 2r'(0) - r'(1) \\ a_3 &= 2[r(0) - r(1)] + r'(0) + r'(1) \end{aligned} \tag{3.9}$$

Implementing these coefficients into the Ferguson equation (3.7) gives

$$\begin{aligned} r(u) =& r(0) + r'(0)u + \{3[r(1) - r(0)] - 2r'(0) - r'(1)\}u^2 \\ &+ \{2[r(0) - r(1)] + r'(0) + r'(1)\}u^3 \end{aligned} \tag{3.10}$$

Rearranging terms

$$r(u) = r(0)H_0 + r(1)H_1 + r'(0)H_2 + r'(1)H_3 \tag{3.11}$$

where H_i are the Hermite polynomials also known as blending functions (see Figure 3.2).

Figure 3.1: Hermite curve specification.

$$
\begin{aligned}
H_0 &= 1 - 3u^2 + 2u^3 \\
H_1 &= 3u^2 - 2u^3 \\
H_2 &= u - 2u^2 + u^3 \\
H_3 &= u^3 - u^2
\end{aligned} \qquad \textbf{(3.12)}
$$

In matrix representation the equation (3.12) becomes

$$
r(u) = \begin{bmatrix} 1 & u & u^2 & u^3 \end{bmatrix} \begin{bmatrix} 1 & 0 & 0 & 0 \\ 0 & 0 & 1 & 0 \\ -3 & 3 & -2 & -1 \\ 2 & -2 & 1 & 1 \end{bmatrix} \begin{bmatrix} r(0) \\ r(1) \\ r\prime(0) \\ r\prime(1) \end{bmatrix} \qquad \textbf{(3.13)}
$$

In short

$$
r(u) = UMG = HG \qquad \textbf{(3.14)}
$$

In here U is a row matrix, M is a Hermite matrix and H is the multiplication of U and M. G is a geometric vector for a one dimensional curve.

Hermite interpolation problem requires a construction of a suitable planar curve fitting for a set of data, which consists of 4 vertex points, 8 tangent vectors and 4 second derivative vectors. The mixed second partial derivative vectors are often called the twist, because large values can cause a corkscrew-like twist at the corners. In here, the twist values are set to zero, which corresponds to a Ferguson surface. The parametric bi-cubic Hermite surface is given by two parameters u and v

$$
r(u,v) = \begin{bmatrix} H_0(u) & H_1(u) & H_2(u) & H_3(u) \end{bmatrix} [C] \begin{bmatrix} H_0(v) \\ H_1(v) \\ H_2(v) \\ H_3(v) \end{bmatrix}, \qquad u,v \in [0,1] \qquad \textbf{(3.15)}
$$

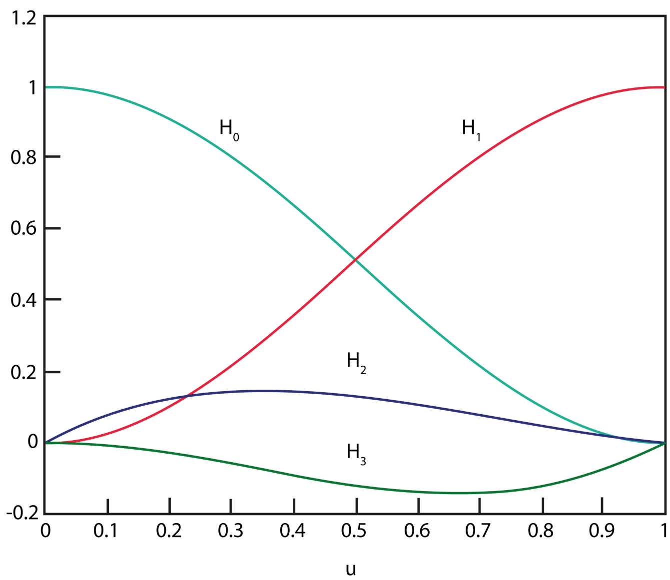

Figure 3.2: Hermite functions.

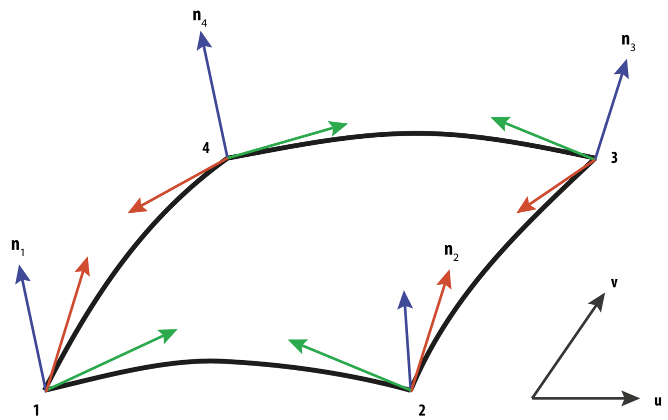

Figure 3.3: 4 vertices and 8 tangent vectors along u and v direction.

where the matrix C is the coefficient matrix

$$[C] = \begin{bmatrix} r(0,0) & r(0,1) & r_v(0,0) & r_v(0,1) \\ r(1,0) & r(1,1) & r_v(1,0) & r_v(1,1) \\ r_u(0,0) & r_u(0,1) & r_{uv}(0,0) & r_{uv}(0,1) \\ r_u(1,0) & r_u(1,1) & r_{uv}(1,0) & r_{uv}(1,1) \end{bmatrix} \tag{3.16}$$

As seen in the Figure 3.3, the coordinates of the vertices are as follows

$$\begin{aligned} r(0,0) &= (x_1, y_1, z_1) \\ r(1,0) &= (x_2, y_2, z_2) \\ r(0,1) &= (x_3, y_3, z_3) \\ r(1,1) &= (x_4, y_4, z_4) \end{aligned} \tag{3.17}$$

And in order to calculate tangent vectors, t_i and s_i are used

$$\mathbf{t}_1 = \begin{bmatrix} x_2 - x_1 \\ y_2 - y_1 \\ z_2 - z_1 \end{bmatrix}, \ \mathbf{t}_2 = \begin{bmatrix} x_1 - x_2 \\ y_1 - y_2 \\ z_1 - z_2 \end{bmatrix}, \ \mathbf{t}_3 = \begin{bmatrix} x_4 - x_3 \\ y_4 - y_3 \\ z_4 - z_3 \end{bmatrix}, \ \mathbf{t}_4 = \begin{bmatrix} x_3 - x_4 \\ y_3 - y_4 \\ z_3 - z_4 \end{bmatrix} \tag{3.18}$$

$$\mathbf{s}_1 = \begin{bmatrix} x_4 - x_1 \\ y_4 - y_1 \\ z_4 - z_1 \end{bmatrix}, \ \mathbf{s}_2 = \begin{bmatrix} x_3 - x_2 \\ y_3 - y_2 \\ z_3 - z_2 \end{bmatrix}, \ \mathbf{s}_3 = \begin{bmatrix} x_2 - x_3 \\ y_2 - y_3 \\ z_2 - z_3 \end{bmatrix}, \ \mathbf{s}_4 = \begin{bmatrix} x_1 - x_4 \\ y_1 - y_4 \\ z_1 - z_4 \end{bmatrix} \tag{3.19}$$

The tangent vector along u direction of point i is calculated from the cross product

$$A_i = \mathbf{n}_i \times \mathbf{t}_i \times \mathbf{n}_i \quad , \quad i = 1,2,3,4 \tag{3.20}$$

The tangent vector along v direction of point i is calculated in a similar manner

$$B_i = \mathbf{n}_i \times \mathbf{s}_i \times \mathbf{n}_i \quad , \quad i = 1,2,3,4 \tag{3.21}$$

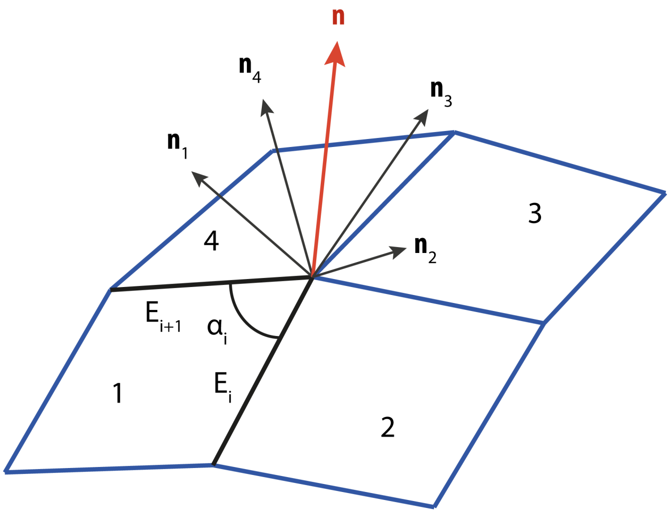

Figure 3.4: Surface normals sharing the same vertex.

Because the values are small, the second derivative vectors are not calculated and they are assumed to be zero. Therefore, this patch is called the Ferguson surface. The C matrix becomes

$$[C] = \begin{bmatrix} r(0,0) & r(0,1) & B_1 & B_3 \\ r(1,0) & r(1,1) & B_2 & B_4 \\ A_1 & A_3 & 0 & 0 \\ A_2 & A_4 & 0 & 0 \end{bmatrix} \tag{3.22}$$

In here, the tangent vectors at vertices are calculated from unique normal vectors at vertices. The calculation of the unique normal vector is given in the next section.

3.2.2 Normal vector computation

If the normal vectors of the quadrilateral element are used for the corresponding vertex, there will be as the same number of normal vectors as the number of elements sharing the same vertex as in the Figure 3.4. But, to provide the continuity along the surface, only one normal vector at each vertex is needed. In order to obtain the normal vectors, the Mean Weighted by Sine and Edge Length Reciprocal (MWSELR) proposed by Max [30] is employed. The six vertex normal calculation algorithms are compared with each other in [31] and the MWSELR algorithm turns out to be the best approach. For comparison, the total drag around a sphere is computed (see section 5.2). For sphere, meshes with 800 and 2400 number of elements (NE) are employed. The result can be seen in the Table 3.1. In MWSELR, the normal vector is given by

$$\mathbf{n} = \sum_{i=1}^{n} \frac{\mathbf{n}_i sin\alpha_i}{|\mathbf{E}_i||\mathbf{E}_{i+1}|} \tag{3.23}$$

Table 3.1: The comparison of vertex normal calculation algorithms.

	NE = 800		NE = 2400	
	TIME	TOTAL DRAG	TIME	TOTAL DRAG
MWSELR	33.224	18.849451323	469.587	18.849541613246
MWE	33.205	18.849450389	469.240	18.849541493966
MWA	33.079	18.849450369	468.857	18.849541495931
MWELR	33.447	18.849451303	474.316	18.849541613244
MWAAT	34.587	18.849440209	476.237	18.849539763241
ANALYTIC	33.224	18.849555921	469.587	18.849555921538

where α_i is the angle between the two edge vectors $\mathbf{E}_i$ and $\mathbf{E}_{i+1}$ of the ith facet sharing the vertex. Information about MWE (Mean Weighted Equally), MWA (Mean Weighted by Angle), MWELR (Mean Weighted by Edge Length Reciprocals) and MWAAT (Mean Weighted by Areas of Adjacent Triangles) may be found in [31].

4. NUMERICAL INTEGRATION

In the preceding chapters the mathematical and numerical formulation of the Stokes flow for boundary integral equation method are derived. Now these integrals have to be evaluated using the quadrature formulas. As can be seen in the equations (3.3) to (3.6), when the source point $\mathbf{x}_0$ gets too close or overlaps with the field point $\mathbf{x}$, the integral becomes singular because of the expression in the denominator. For these singular integrals $tanh - sinh$ quadrature rule proposed by Takahasi and Mori [12] is used. And for the non-singular ones the classical Gaussian quadrature method is applied.

4.1 Evaluation of Non-Singular Integrals

Any quadrature rule approximates a definite integral of a function using the sum of weights at specified points on the solution domain. One of the most popular quadrature rule is the Gaussian quadrature formula introduced by Carl Friedrich Gauss.

4.1.1 The Gaussian quadrature rule

The details of the Gaussian quadrature rule can be found in [32], [33] and [34]. The basis of this method is the trapezoidal rule which was developed by the method of undetermined coefficients

$$\int_a^b f(x)dx \approx c_1 f(a) + c_2 f(b) = \frac{b-a}{2} f(a) + \frac{b-a}{2} f(b) \qquad \textbf{(4.1)}$$

In the Gaussian quadrature method the arguments a and b are not explicit, they are unknowns

$$\int_a^b f(x)dx \approx w_1 f(x_1) + w_2 f(x_2) \qquad \textbf{(4.2)}$$

Hence there are four unknowns: the weights w_1 and w_2 and the arguments x_1 and x_2. Therefore, the polynomial has to be third order to have four unknowns

$$f(x) = a_0 + a_1 x + a_2 x^2 + a_3 x^3 \qquad \textbf{(4.3)}$$

Integrating these function from a to b yields

$$\begin{aligned}\int_a^b f(x)dx &= \int_a^b [a_0 + a_1 x + a_2 x^2 + a_3 x^3]dx \\ &= \left[a_0 x + a_1 \frac{x^2}{2} + a_2 \frac{x^3}{3} + a_3 \frac{x^4}{4}\right]_a^b \\ &= a_0(b-a) + a_1 \frac{b^2-a^2}{2} + a_2 \frac{b^3-a^3}{3} + a_3 \frac{b^4-a^4}{4}\end{aligned} \tag{4.4}$$

Also the right hand side of the equation (4.2) becomes

$$w_1[a_0 + a_1 x_1 + a_2 x_1^2 + a_3 x_1^3] + w_2[a_0 + a_1 x_1 + a_2 x_1^2 + a_3 x_1^3] \tag{4.5}$$

Rewriting this expression

$$a_0(w_1 + w_2) + a_1(w_1 x_1 + w_2 x_2) + a_2(w_1 x_1^2 + w_2 x_2^2) + a_3(w_1 x_1^3 + w_2 x_2^3) \tag{4.6}$$

and equating the equations (4.4) and (4.6) results in four equations for four unknowns

$$w_1 + w_2 = b - a \tag{4.7}$$

$$w_1 x_1 + w_2 x_2 = \frac{b^2 - a^2}{2} \tag{4.8}$$

$$w_1 x_1^2 + w_2 x_2^2 = \frac{b^3 - a^3}{3} \tag{4.9}$$

$$w_1 x_1^3 + w_2 x_2^3 = \frac{b^4 - a^4}{4} \tag{4.10}$$

Note that except the equation (4.7), the equations above are non-linear and the system can not be solved explicitly. After a trial and error methodology the only acceptable solution is as follows

$$\begin{aligned} w_1 &= \frac{b-a}{2} \\ w_2 &= \frac{b-a}{2} \\ x_1 &= \left(\frac{b-a}{2}\right)\left(-\frac{1}{\sqrt{3}}\right) + \frac{b+a}{2} \\ x_2 &= \left(\frac{b-a}{2}\right)\left(\frac{1}{\sqrt{3}}\right) + \frac{b+a}{2}\end{aligned} \tag{4.11}$$

Generally the Gaussian quadratures are given in the interval of $[-1,1]$ therefore, the integration limits $[a,b]$ have to be transformed

$$\int_a^b f(x)dx = \int_{-1}^1 g(\varphi)d\varphi \tag{4.12}$$

In order to do that, the following transformation is used

$$x = m\varphi + c \tag{4.13}$$

Here m is to contract or expand while c is to translate the interval of the integration. When $x = a$, φ is to be -1 and when $x = b$, φ is to be 1

$$\begin{aligned} a &= m(-1) + c \\ b &= m(1) + c \end{aligned} \tag{4.14}$$

Solving the system gives

$$\begin{aligned} m &= \frac{b-a}{2} \\ c &= \frac{b+a}{2} \end{aligned} \tag{4.15}$$

and

$$\begin{aligned} x &= \frac{b-a}{2}\varphi + \frac{b+a}{2} \\ dx &= \frac{b-a}{2}d\varphi \end{aligned} \tag{4.16}$$

Substituting these expressions into the original equation (4.12)

$$\int_a^b f(x)dx = \int_{-1}^{1} f\left(\frac{b-a}{2}\varphi + \frac{b+a}{2}\right)\frac{b-a}{2}d\varphi \tag{4.17}$$

Now substitute the values [-1,1] into the equation (4.11) for [a,b]

$$\begin{aligned} w_1 &= 1 \\ w_2 &= 1 \\ x_1 &= -0.577350269 \\ x_2 &= 0.577350269 \end{aligned} \tag{4.18}$$

These are the weights and points (arguments) for the two-point ($n = 2$) Gaussian quadrature rule. For n points, the weights and points can be found in the same way using $2n-1$ degree polynomial for the equation (4.3). The polynomials used here are Legendre polynomials. As a result the n point *Gauss-Legendre* quadrature rule becomes

$$\int_{-1}^{1} f(x)dx = \sum_{i=1}^{n} w_i f(x_i) \tag{4.19}$$

The weights and points for n up to 10 can be found in Appendix A.

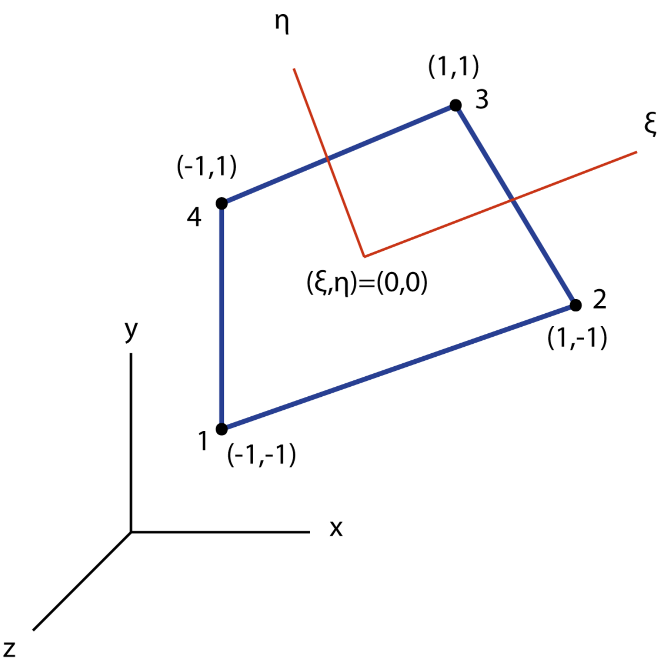

Figure 4.1: Quadrilateral element with local coordinates ξ and η.

4.1.2 Application of the Gauss-Legendre quadratures to non-singular integrals

In order to evaluate integrals in the equations (3.3) to (3.4) the following relations are used

$$\iint_{S_B} f dS = \int_{-1}^{1}\int_{-1}^{1} f(\xi,\eta)|J|d\xi d\eta \tag{4.20}$$

Here J is the Jacobian matrix, ξ and η are the local coordinate axis of the quadrilateral element as seen in the Figure 4.1. The Jacobian of the transformation is given by

$$|J| \quad = \quad \left| \begin{Bmatrix} \frac{\partial x}{\partial \xi} \\ \frac{\partial y}{\partial \xi} \\ \frac{\partial z}{\partial \xi} \end{Bmatrix} \times \begin{Bmatrix} \frac{\partial x}{\partial \eta} \\ \frac{\partial y}{\partial \eta} \\ \frac{\partial z}{\partial \eta} \end{Bmatrix} \right| \tag{4.21}$$

The unknown traction vector components are represented using the bilinear interpolations over the quadrilateral elements

$$\mathbf{t}(\xi,\eta) \quad = \quad \sum_{j=1}^{4} \mathbf{t}_j N_j(\xi,\eta) \tag{4.22}$$

and the shape functions are given by

$$N_j(\xi,\eta) \quad = \quad \frac{(1+\xi\xi_j)(1+\eta\eta_j)}{4} \tag{4.23}$$

Now the equation (3.3) becomes

$$
\begin{aligned}
8\pi\mu u_1(\mathbf{x}) &= \sum_{k=1}^{NE}\int_{-1}^{1}\int_{-1}^{1}\left[\sum_{m=1}^{4} t_{1mk}(\xi,\eta)N_m(\xi,\eta)\right]S_{11}|J|d\xi d\eta \\
&+\sum_{k=1}^{NE}\int_{-1}^{1}\int_{-1}^{1}\left[\sum_{m=1}^{4} t_{2mk}(\xi,\eta)N_m(\xi,\eta)\right]S_{12}|J|d\xi d\eta \\
&+\sum_{k=1}^{NE}\int_{-1}^{1}\int_{-1}^{1}\left[\sum_{m=1}^{4} t_{3mk}(\xi,\eta)N_m(\xi,\eta)\right]S_{13}|J|d\xi d\eta
\end{aligned}
\tag{4.24}
$$

Applying n point Gauss-Legendre quadrature to this expression yields

$$
\begin{aligned}
8\pi\mu u_1(\mathbf{x}) &= \sum_{k=1}^{NE}\sum_{i=1}^{n}\sum_{j=1}^{n}\sum_{m=1}^{4} t_{1mk}\left[\frac{1}{r}+\frac{(x_1-x_{0_1})^2}{r^3}\right]N_m(\xi_i,\eta_j)|J|w_iw_j \\
&+\sum_{k=1}^{NE}\sum_{i=1}^{n}\sum_{j=1}^{n}\sum_{m=1}^{4} t_{2mk}\left[\frac{(x_1-x_{0_1})(x_2-x_{0_2})}{r^3}\right]N_m(\xi_i,\eta_j)|J|w_iw_j \\
&+\sum_{k=1}^{NE}\sum_{i=1}^{n}\sum_{j=1}^{n}\sum_{m=1}^{4} t_{3mk}\left[\frac{(x_1-x_{0_1})(x_3-x_{0_3})}{r^3}\right]N_m(\xi_i,\eta_j)|J|w_iw_j
\end{aligned}
\tag{4.25}
$$

In a similar manner, y- and z-component of the velocity are as follows

$$
\begin{aligned}
8\pi\mu u_2(\mathbf{x}) &= \sum_{k=1}^{NE}\sum_{i=1}^{n}\sum_{j=1}^{n}\sum_{m=1}^{4} t_{1mk}\left[\frac{(x_2-x_{0_2})(x_1-x_{0_1})}{r^3}\right]N_m(\xi_i,\eta_j)|J|w_iw_j \\
&+\sum_{k=1}^{NE}\sum_{i=1}^{n}\sum_{j=1}^{n}\sum_{m=1}^{4} t_{2mk}\left[\frac{1}{r}+\frac{(x_2-x_{0_2})^2}{r^3}\right]N_m(\xi_i,\eta_j)|J|w_iw_j \\
&+\sum_{k=1}^{NE}\sum_{i=1}^{n}\sum_{j=1}^{n}\sum_{m=1}^{4} t_{3mk}\left[\frac{(x_2-x_{0_2})(x_3-x_{0_3})}{r^3}\right]N_m(\xi_i,\eta_j)|J|w_iw_j
\end{aligned}
\tag{4.26}
$$

$$
\begin{aligned}
8\pi\mu u_3(\mathbf{x}) &= \sum_{k=1}^{NE}\sum_{i=1}^{n}\sum_{j=1}^{n}\sum_{m=1}^{4} t_{1mk}\left[\frac{(x_3-x_{0_3})(x_1-x_{0_1})}{r^3}\right]N_m(\xi_i,\eta_j)|J|w_iw_j \\
&+\sum_{k=1}^{NE}\sum_{i=1}^{n}\sum_{j=1}^{n}\sum_{m=1}^{4} t_{2mk}\left[\frac{(x_3-x_{0_3})(x_2-x_{0_2})}{r^3}\right]N_m(\xi_i,\eta_j)|J|w_iw_j \\
&+\sum_{k=1}^{NE}\sum_{i=1}^{n}\sum_{j=1}^{n}\sum_{m=1}^{4} t_{3mk}\left[\frac{1}{r}+\frac{(x_3-x_{0_3})^2}{r^3}\right]N_m(\xi_i,\eta_j)|J|w_iw_j
\end{aligned}
\tag{4.27}
$$

And the pressure is

$$\begin{aligned}8\pi P(\mathbf{x}) = &\sum_{k=1}^{NE}\sum_{i=1}^{n}\sum_{j=1}^{n}\sum_{m=1}^{4} t_{1mk}\left[2\frac{(x_1-x_{0_1})}{r^3}\right] N_m(\xi_i,\eta_j)|J|w_i w_j \\ &+\sum_{k=1}^{NE}\sum_{i=1}^{n}\sum_{j=1}^{n}\sum_{m=1}^{4} t_{2mk}\left[2\frac{(x_2-x_{0_2})}{r^3}\right] N_m(\xi_i,\eta_j)|J|w_i w_j \\ &+\sum_{k=1}^{NE}\sum_{i=1}^{n}\sum_{j=1}^{n}\sum_{m=1}^{4} t_{3mk}\left[2\frac{(x_3-x_{0_3})}{r^3}\right] N_m(\xi_i,\eta_j)|J|w_i w_j\end{aligned} \tag{4.28}$$

The field points $\mathbf{x}$ in the equations are computed using the Hermite interpolation surfaces on the quadrilateral elements.

4.2 Evaluation of Singular Integrals

There are several methods for the evaluation of singular integrals in the literature. In the spectral element method of Muldowney and Higdon [7], the best method is found to be the variable mapping that cluster quadrature points close to the singularity point. Let x_i and x_j be the classical Gauss-Legendre points and s_i and t_j be the new shifted points. Then the mapped variables on the local coordinates become

$$\xi_i\left(\frac{sinh\beta s_i}{sinh\beta}\right)^2 \quad , \quad \eta_j\left(\frac{sinh\beta t_j}{sinh\beta}\right)^2 \tag{4.29}$$

In here β is an empirical parameter and $\beta = 4$ gives the best results.
Another method was developed by Duffy for pyramids and cubes [9], Muosavi and Sukumar [10] improve the technique for two dimensional surface elements using a transformation from triangular element to unit square (see Figure 4.2) using the mapping $x = u^\beta$ and $y = u^\beta v^\gamma$ which gives

$$I = \int_0^1 dx \int_0^1 dy \frac{f(x,y)}{(x^2+y^2)^{\lambda/2}} = \int_0^1\int_0^1 \frac{f(u^\beta, u^\beta v^\gamma)}{[u^{2\beta}(1+v^{2\gamma})]^{\lambda/2}} J du dv \tag{4.30}$$

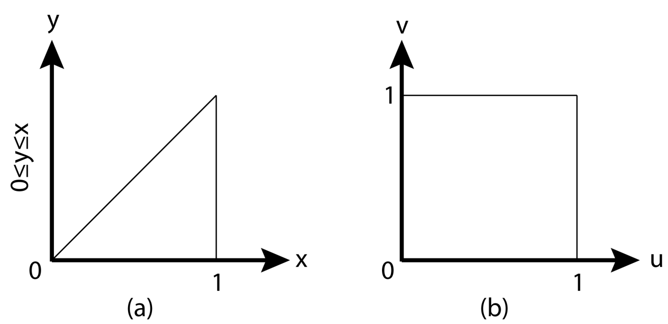

Figure 4.2: Transformation of standard triangle (a) into unit square (b).

where $J = \beta\gamma u^{2\beta-1}v^{\gamma-1}$. Here $\lambda \neq 0$ is the strength of singularity. β and γ are chosen in order to make the transformed kernel smooth and integrable with the fewest number of evaluation points. After this mapping triangles with a vertex singularity is transformed in a way that the singularity is moved to the origin. Then affine map to the standard triangle is used

$$\begin{aligned} x &= aX + bY \\ y &= cX + dY \end{aligned} \tag{4.31}$$

In here (X,Y) is the physical coordinate system of arbitrary triangle whereas (x,y) is the plane of standard triangle.

4.2.1 *tanh-sinh* quadrature rule

The $tanh - sinh$ quadrature method is based on the use of appropriate mapping functions to change the finite interval $[a,b]$ into the interval of $[-\infty,+\infty]$ [12]. The transformation is applied as follows for a given integral

$$I = \int_a^b f(x)dx \tag{4.32}$$

Now define a transformation such as

$$\begin{aligned} x &= \phi(u) \\ dx &= \phi'(u) \end{aligned} \tag{4.33}$$

where $\phi(-\infty) = a$ and $\phi(+\infty) = b$ therefore, the interval $[a,b]$ is changed into $[-\infty,+\infty]$ and the integral becomes

$$I = \int_{-\infty}^{+\infty} f[\phi(u)]\phi'(u) \tag{4.34}$$

The important point on choosing the mapping function is that $g(u)$ has to be a decay property as follows

$$g(u) \approx exp\left(-\frac{\pi}{2}exp|u|\right), \qquad u \to \pm\infty \tag{4.35}$$

Using this property, a mapping function for $[a,b]$ to $[-\infty,+\infty]$ is proposed such as

$$\begin{aligned} x &= tanh\left(\frac{\pi}{2}sinh(u)\right) \\ dx &= sech^2\left(\frac{\pi}{2}sinh(u)\right)\frac{\pi}{2}cosh(u) \end{aligned} \tag{4.36}$$

where

$$sech^2\left(\frac{\pi}{2}sinh(u)\right) = \frac{1}{cosh^2\left(\frac{\pi}{2}sinh(u)\right)} \tag{4.37}$$

Substituting these into the equation (4.32)

$$I = \int_{-\infty}^{+\infty} f\left[tanh\left(\frac{\pi}{2}sinh(u)\right)\right] \frac{\frac{\pi}{2}cosh(u)}{cosh^2\frac{\pi}{2}sinh(u)} \tag{4.38}$$

Applying the trapezoidal rule with mesh size h, the equation (4.38) yields

$$I = h\sum_{j=-\infty}^{+\infty} f\left[tanh\left(\frac{\pi}{2}sinh(jh)\right)\right] \frac{\frac{\pi}{2}cosh(jh)}{cosh^2\frac{\pi}{2}sinh(jh)} \tag{4.39}$$

In here, the quadrature points and weights are as follows respectively

$$x_j = tanh\left(\frac{\pi}{2}sinhjh\right) \tag{4.40}$$

$$w_j = \frac{\frac{\pi}{2}coshjh}{cosh^2(\frac{\pi}{2}sinhjh)} \tag{4.41}$$

The schematic representations of quadrature points and weights for the Gauss-Legendre and $tanh-sinh$ method for $n=4$ and $m=2$, respectively, are shown in the Figure 4.3. As it may seen, the points for $tanh-sinh$ quadrature are stretched to the corners in order to avoid singularities at vertices. The weights for 21×21 points on a quadrilateral element are presented in The Figure 4.3(b).

The $tanh-sinh$ scheme is based on the Euler- MacLaurin summation formula which is an asymptotic error analysis for trapezoidal rule, a more detailed information can be foun in [35]. If $\phi'(u)$ and its derivatives goes to zero fast enough for large $|t|$ then, the equation (4.34) will be a smooth function although $f(x)$ has singularities at endpoints [36]. Because of the $cosh^2$ term in the denominator of the equation (4.41) this method is called the *double exponential formula*, the mapping function has the property of decaying at a double exponential rate at infinity [37].

4.2.2 The numerical algorithm for *tanh-sinh* quadrature

In the preceding section the points and weights for $tanh-sinh$ quadrature rule are derived. The adaptation of this formulas to the evaluation of integrals is done by using the algorithm proposed in [36], the pseudo code for the algorithm can be found in Appendix B. In the equations (4.40) and (4.41), h is the mesh step size and it is set to $h=2^{-m}$, where m is the level of the algorithm. We set m to different values from 2 to 4 depending on the accuracy of problem. The values of the weights and point for $m=1$ to $m=4$ can be found in Table B.1.

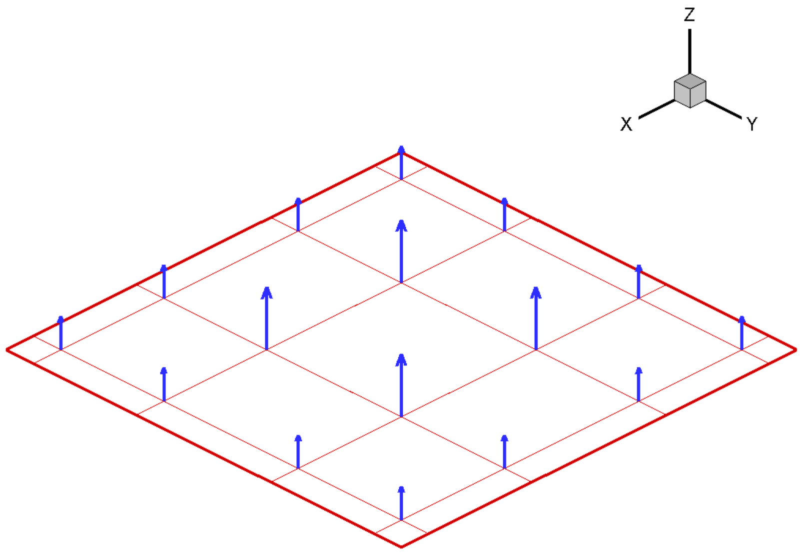

(a) Gauss-Legendre.

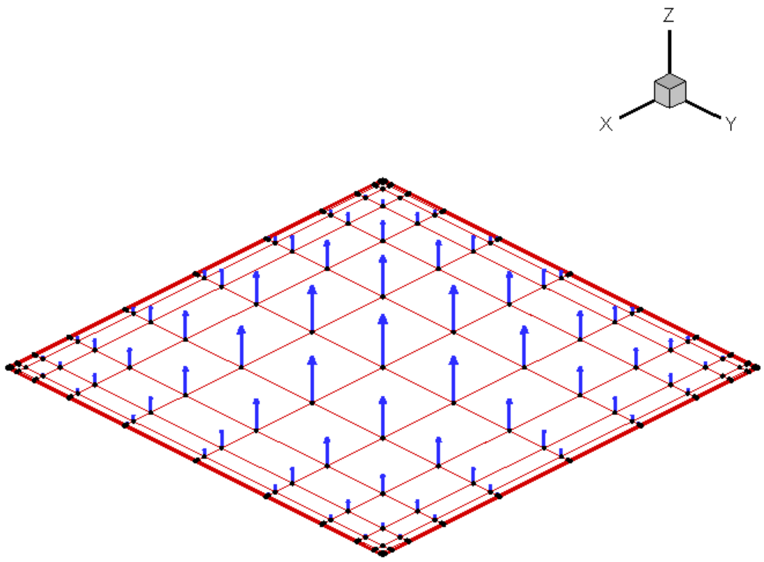

(b) *tanh-sinh*.

Figure 4.3: The Gauss-Legendre (a) and *tanh-sinh* (b) quadrature points with weights on quadrilateral element.

5. NUMERICAL RESULTS

In this section, the numerical algorithm is initially validated for the three-dimensional unbounded Stokes flow around a sphere. Then the algorithm is applied to the sedimentation of spherical particles. All the computations are done by a desktop PC with an Intel(R) Core(TM) i7-3770 340 GHz processor and 16 GB memory.

5.1 The Exact Solution of the Stokes Flow around a Sphere

The derivation of the solution of the Stokes flow around a sphere can be found in the textbooks [38] and [39]. A sphere with radius R is shown in the Figure 5.1. Flow around the sphere is axisymmetric and the flow does not change in the direction of θ and ϕ.

$$\nabla \times (\nabla P) = \mu \nabla \times (\nabla^2 \mathbf{u}) \tag{5.1}$$

Recall that the curl of a gradient is zero. In addition the curl and ∇^2 operators are interchangeable. Using the continuity equation

$$\mu \nabla^2 \omega = 0 \tag{5.2}$$

where ω is the vorticity. The vorticity in the spherical coordinates for an axisymmetric problems is given by

$$\omega_\phi = \frac{1}{r}\left[\frac{\partial (r u_\theta)}{\partial r} - \frac{\partial u_r}{\partial \theta}\right] \tag{5.3}$$

In the spherical coordinates the velocity components are defined as

$$\begin{aligned} u_r &= \frac{1}{r^2 sin\theta}\frac{\partial \psi}{\partial \theta} \\ u_\theta &= -\frac{1}{r sin\theta}\frac{\partial \psi}{\partial r} \end{aligned} \tag{5.4}$$

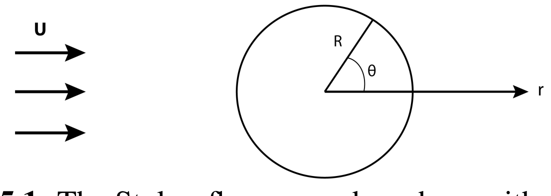

Figure 5.1: The Stokes flow around a sphere with radius R.

where ψ is the stream function. Inserting the equation (5.4) into the equation (5.3) the vorticity is derived in terms of the stream function

$$\omega_\phi = -\frac{1}{r}\left[\frac{1}{sin\theta}\frac{\partial^2\psi}{\partial r^2} + \frac{1}{r^2}\frac{\partial}{\partial\theta}\left(\frac{1}{sin\theta}\frac{\partial\psi}{\partial\theta}\right)\right] \tag{5.5}$$

Inserting this relation into the equation (5.2)

$$\left[\frac{\partial^2}{\partial r^2} + \frac{sin\theta}{r^2}\frac{\partial}{\partial\theta}\left(\frac{1}{sin\theta}\frac{\partial}{\partial\theta}\right)\right]^2 \psi = 0 \tag{5.6}$$

The boundary condition on the sphere is no-slip boundary condition and the velocities on the surface are zero. At the far-field of the sphere, the velocity is equal to U. Therefore the boundary conditions are as follows

$$\begin{aligned} \psi(R,\theta) &= 0 \\ \frac{\partial\psi}{\partial r}(R,\theta) &= 0 \\ \psi(\infty,\theta) &= \frac{1}{2}Ur^2 sin^2\theta \end{aligned} \tag{5.7}$$

The third condition suggests a solution in the following form

$$\psi = f(r) sin^2\theta \tag{5.8}$$

Inserting into the equation (5.6) yields

$$f'''' - \frac{4f''}{r^2} + \frac{8f'}{r^3} - \frac{8f}{r^4} = 0 \tag{5.9}$$

which has a solution

$$f = Ar^4 + Br^2 + Cr + \frac{D}{r} \tag{5.10}$$

Applying this solution to the third boundary condition

$$\left[Ar^4 + Br^2 + Cr + \frac{D}{r}\right] sin^2\theta = \frac{1}{2}Ur^2 sin^2\theta \quad as \quad r \to \infty \tag{5.11}$$

gives the coefficients $A = 0$ and $B = U/2$. Now applying the relation (5.10) into the first and second boundary conditions

$$\begin{aligned} \psi(R,\theta) &= \left[\frac{U}{2}R^2 + CR + \frac{D}{R}\right] sin^2\theta = 0 \\ \frac{\partial\psi}{\partial r}(R,\theta) &= \left[2\frac{U}{2}R + C - \frac{D}{R^2}\right] sin^2\theta = 0 \end{aligned} \tag{5.12}$$

Solving the system gives

$$C = -\frac{3UR}{4} \quad and \quad D = \frac{UR^3}{4} \tag{5.13}$$

Therefore, the stream function and the velocity components become

$$\psi = Ur^2 sin^2\theta \left[\frac{1}{2} - \frac{3R}{4r} + \frac{R^3}{4r^3}\right] \quad \textbf{(5.14)}$$

$$u_r = Ucos\theta \left[1 - \frac{3R}{2r} + \frac{R^3}{2r^3}\right] \quad \textbf{(5.15)}$$

$$u_\theta = -Usin\theta \left[1 - \frac{3R}{4r} - \frac{R^3}{4r^3}\right] \quad \textbf{(5.16)}$$

Due to the axisymmetry of the flow, the variations in the ϕ direction disappears. Therefore, the momentum equation (2.10) can be written in the following form

$$\begin{bmatrix} \dfrac{\partial P}{\partial r} \\ \dfrac{\partial P}{\partial \theta} \end{bmatrix} = \mu \begin{bmatrix} \nabla^2 u_r - \dfrac{2u_r}{r^2} - \dfrac{2}{r^2 sin\theta}\dfrac{\partial}{\partial\theta}(u_\theta sin\theta) \\ \nabla^2 u_\theta - \dfrac{u_\theta}{r^2 sin^2\theta} + \dfrac{2}{r^2}\dfrac{\partial u_r}{\partial\theta} \end{bmatrix} \quad \textbf{(5.17)}$$

In here, ∇^2 is given in the spherical coordinates for (r,θ)

$$\nabla^2 = \frac{1}{r^2}\frac{\partial}{\partial r}\left(r^2\frac{\partial}{\partial r}\right) + \frac{1}{r^2 sin\theta}\frac{\partial}{\partial\theta}\left(sin\theta\frac{\partial}{\partial\theta}\right) \quad \textbf{(5.18)}$$

Inserting the equations (5.15) and (5.16) into the equation (5.17), the first equation becomes

$$\begin{aligned} \frac{\partial P}{\partial r} = Ucos\theta\frac{3R^3}{r^5} &- \frac{2Ucos\theta}{r^2}\left[1 - \frac{3R}{2r} + \frac{r^3}{2r^3}\right] \\ &- \frac{2Ucos\theta}{r^2}\left[1 - \frac{3R}{2r} + \frac{r^3}{2r^3}\right] \\ &+ \frac{4Ucos\theta}{r^2}\left[1 - \frac{3R}{4r} - \frac{R^3}{4r^3}\right] \end{aligned} \quad \textbf{(5.19)}$$

Rearranging the above equations gives

$$\frac{\partial P}{\partial r} = Ucos\theta\frac{3R}{r^3} \quad \textbf{(5.20)}$$

The integration of the equation (5.20) from $r = 0$ to $r = \infty$ gives the pressure

$$P = -\frac{3R\mu Ucos\theta}{2r^2} + P_\infty \quad \textbf{(5.21)}$$

In order to calculate the drag D on the sphere, the stress over the surface of the sphere is integrated. The stress tensor for a Newtonian fluid is as follows

$$\sigma_{ij} = -P\delta_{ij} + \varepsilon_{ij} \quad \textbf{(5.22)}$$

where ε is the viscous stress tensor. In the spherical coordinates it becomes

$$\begin{aligned} \varepsilon_{rr} &= 2\mu\frac{\partial u_r}{\partial r} = 2\mu Ucos\theta\left[\frac{3R}{2r^2} - \frac{3R^3}{2r^4}\right] \\ \varepsilon_{r\theta} &= \mu\left[r\frac{\partial}{\partial r}\left(\frac{u_\theta}{r}\right) + \frac{1}{r}\frac{\partial u_r}{\partial\theta}\right] = -3\mu Usin\theta\left[\frac{R^3}{2r^4}\right] \end{aligned} \quad \textbf{(5.23)}$$

Then the r-component of the drag force per unit area on the sphere surface is given by

$$-Pcos\theta + \varepsilon_{rr}cos\theta - \varepsilon_{r\theta}sin\theta \quad \textbf{(5.24)}$$

Substituting the relations (5.21) and (5.23) into the equation (5.24) the hydrodynamic traction vector on the sphere surface becomes

$$\mathbf{t} = \frac{3\mu}{2R}U \quad \textbf{(5.25)}$$

And the total drag around the sphere of radius R with the sphere velocity U is found by multiplying this traction vector with the surface area of the sphere $4\pi R^2$

$$D = 6\pi\mu UR \quad \textbf{(5.26)}$$

5.2 The Numerical Solution of the Unbounded Stokes Flow around a Sphere

In this case, the free stream velocity is set to $\mathbf{U}(x,y,x) = (1,0,0)$, the sphere moves along the positive x-direction with a speed of unity. The radius R is taken to be 1. The viscosity is taken to be unity, therefore the total drag is computed to be

$$D = 6\pi = 18.849555921538 \quad \textbf{(5.27)}$$

Using the equations (4.25) to (4.28), a set of algebraic equations are constructed as follows

$$[A]\{t\} = \{u\} \quad \textbf{(5.28)}$$

In here t is the traction, u is the velocity on the surface of the sphere. The size of the A matrix is $(3 \times NP) \times (3 \times NP)$. The boundary condition on the sphere is no-slip. The linear system is solved using the direct solver within the Intel Math Kernel Library.

Although the computed total drag is not a good measure of solution accuracy, it is used to validate the present integral equation flow solver. For the present benchmark problem three meshes are employed: the coarse mesh with 1410 nodes and 1408 elements, the medium mesh with 2402 nodes and 2400 elements and the fine mesh with 5402 nodes and 5400 elements. The computational quadrilateral surface meshes are shown in the Figure 5.2. The computed local traction vectors are shown in the Figure 5.3. The computed total drag values are tabulated in the Table 5.1 and compared with the analytical exact value. The converge analysis of the error indicates an algebraic convergence rate of $O(\Delta h^3)$.

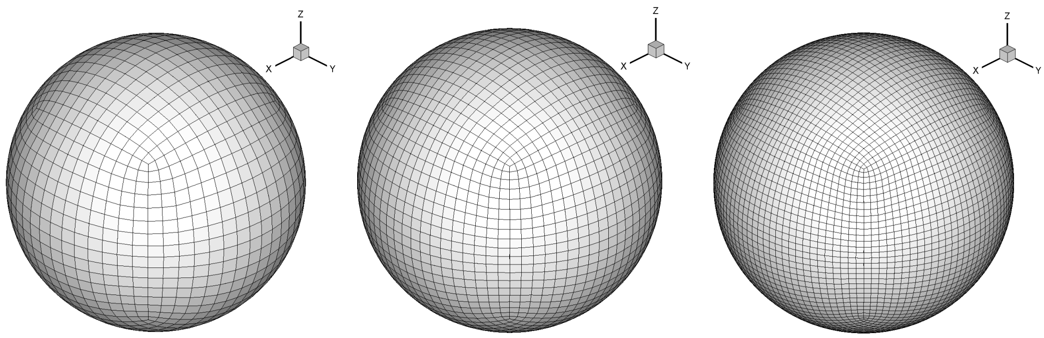

Figure 5.2: The computational mesh with element numbers 1408 (left), 2400 (middle) and 5400 (right).

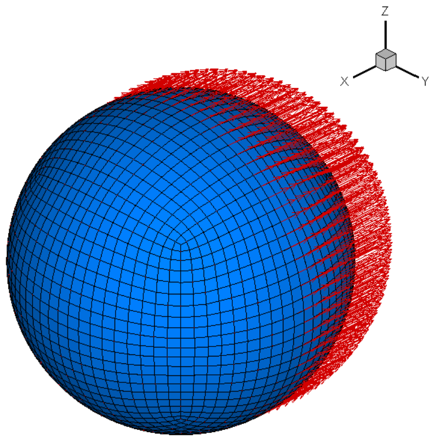

Figure 5.3: Traction vectors on the sphere moving along x axis.

5.3 Sedimentation of Spherical Particles

The equations of motion that are used in the algorithm for free falling spheres are as follows

$$\sum \mathbf{F} = \frac{d}{dt}(m\dot{\mathbf{x}}) = m\frac{d\mathbf{u}}{dt} \tag{5.29}$$

$$\sum \mathbf{M} = \frac{d}{dt}(I\dot{\boldsymbol{\theta}}) = I\frac{d\boldsymbol{\omega}}{dt} \tag{5.30}$$

where m is the mass, $\mathbf{u}$ is the linear velocity, I is the moment of inertia and $\boldsymbol{\omega}$ is the angular velocity. If the time derivation is discretized using the first-order backward

Table 5.1: The convergence of the total drag for the Stokes flow past sphere.

NE	Total Drag (Numerical)	Error
5400	18.849552908422041	3.013116 e-06
2400	18.849545680592303	1.024094 e-05
1408	18.849533161883699	2.275965 e-05

differencing, the linear momentum equations become

$$
\begin{aligned}
\oiint_{S_B} t_x dS &= m\frac{u^{n+1}-u^n}{\Delta t} \\
-mg+\oiint_{S_B} t_y dS &= m\frac{v^{n+1}-u^n}{\Delta t} \\
\oiint_{S_B} t_z dS &= m\frac{w^{n+1}-w^n}{\Delta t}
\end{aligned}
\tag{5.31}
$$

and the angular momentum equations become

$$
\begin{aligned}
\oiint_{S_B} (r\times t)_x dS &= I_x\frac{\omega_x^{n+1}-\omega_x^n}{\Delta t} \\
\oiint_{S_B} (r\times t)_y dS &= I_y\frac{\omega_y^{n+1}-\omega_y^n}{\Delta t} \\
\oiint_{S_B} (r\times t)_z dS &= I_z\frac{\omega_z^{n+1}-\omega_z^n}{\Delta t}
\end{aligned}
\tag{5.32}
$$

The boundary condition on the sphere surface can be written as follows

$$
\mathbf{u}(\mathbf{x}_0) = \mathbf{U} + \boldsymbol{\omega}\times\mathbf{r}
\tag{5.33}
$$

where $\mathbf{u}$ is the velocity at the collocation point $\mathbf{x}_0$, $\mathbf{U}$ and $\boldsymbol{\omega}$ are the linear and angular velocities of the sphere centroid, respectively, and $\mathbf{r}$ is the position vector $\mathbf{x}_0$ relative to the centre of gravity. Then the system of algebraic equations can be constructed in the following form

$$
\left[\begin{array}{c|c}
A & B \\
\hline
C & D
\end{array}\right]
\left[\begin{array}{c}
t_{1_x} \\ t_{1_y} \\ t_{1_z} \\ \vdots \\ t_{NP_x} \\ t_{NP_y} \\ t_{NP_z} \\ \hline U_1^{n+1} \\ \omega_1^{n+1} \\ \vdots \\ U_{NB}^{n+1} \\ \omega_{NB}^{n+1}
\end{array}\right]
=
\left[\begin{array}{c}
0 \\ 0 \\ 0 \\ \vdots \\ 0 \\ 0 \\ 0 \\ \hline U_1^n(m/\Delta t) \\ \omega_1^n(I/\Delta t) \\ \vdots \\ U_{NB}^n(m/\Delta t) \\ \omega_{NB}^n(I/\Delta t)
\end{array}\right]
\tag{5.34}
$$

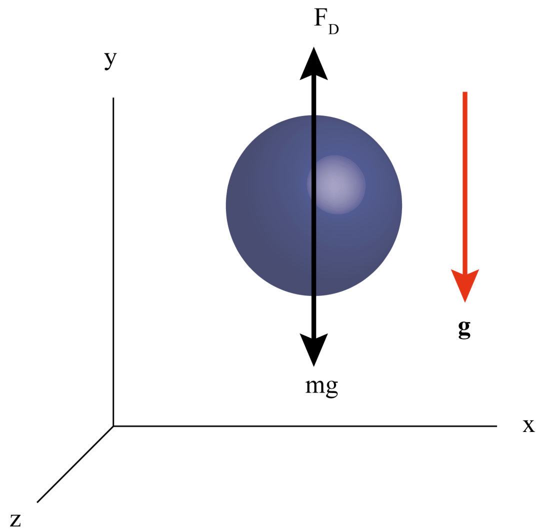

Figure 5.4: Sphere in free fall.

where NB is the number of bodies in the flow. In here, the local matrix A is the same matrix in the equation (5.28), the local matrix B is the coefficient matrix which is constructed from following equations

$$\begin{aligned} u_1 - U_1 - (\omega_y r_z - \omega_z r_y) &= 0 \\ u_2 - U_2 - (\omega_z r_x - \omega_x r_z) &= 0 \\ u_3 - U_3 - (\omega_x r_y - \omega_y r_x) &= 0 \end{aligned} \tag{5.35}$$

Thus the local matrix B has a dimension of $(6 \times NP)$ for a single sphere. The local matrices C and D has 6 rows for a single sphere, of which 3 rows are for the linear momentum and 3 rows are for the angular momentum equations. In here, the local matrix C is computed from surface integration. The local matrix D is a diagonal matrix. In this section, initially a single sphere falling in an unbounded domain is numerically investigated. Then the algorithm is applied to the cluster of two and three spheres in free fall.

5.3.1 One sphere in free fall

For the present problem (see Figure 5.4), the radius of the sphere R is again 1, but the mass of the sphere is chosen to set

$$m\mathbf{g} = F_D = 18.849555921538 \tag{5.36}$$

Therefore the terminal velocity of the sphere is expected to be 1 after some time. Therefore the mass is equal to 1.921463397. The calculations are started from the rest with a time step of 0.005. The time variation of the sphere free fall velocity is

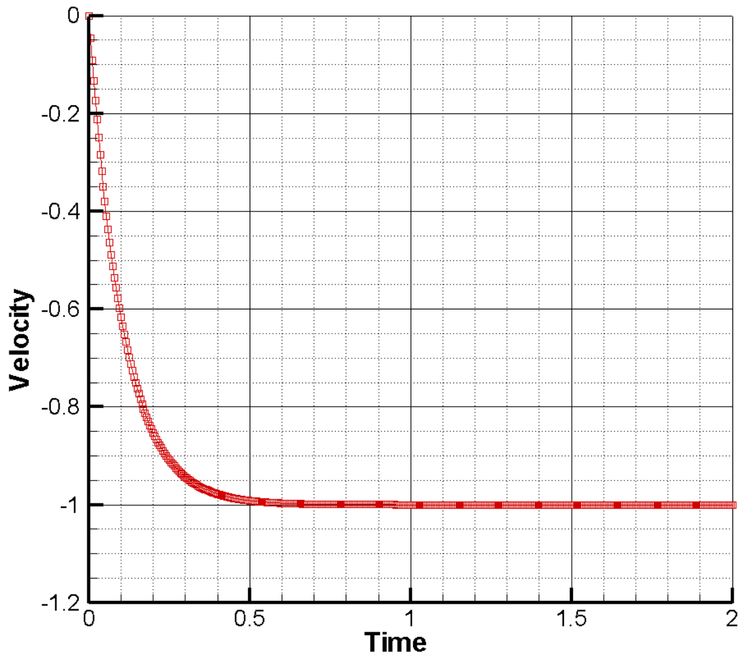

Figure 5.5: The time variation of the sphere velocity falling in an unbounded domain.

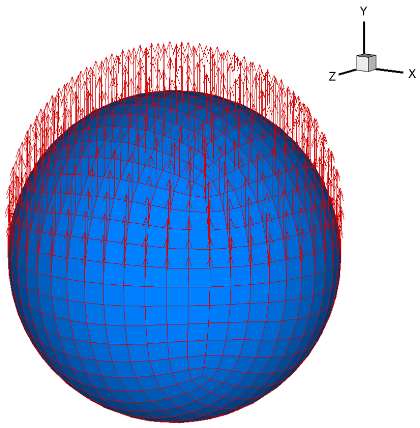

Figure 5.6: Traction vector on falling sphere with terminal velocity.

shown in the Figure 5.5 and the sphere reaches the terminal velocity of 1 after $t = 0.6$. The traction vectors for terminal velocity can be seen in the Figure 5.6.

5.3.2 Two spheres in free fall

In the second case, the trajectories of two spheres are calculated. The benchmark problem was proposed in the work of Ingber and Mammoli [40]. The problem consists of two identical spheres in free fall with a 45^o angle between their line of centres as shown in the Figure 5.7. The gap between spheres ε is set to $0.1R$. The comparison of the results for U_v/U_t and U_h/U_t is shown in the Tables 5.2 and 5.3, where U_t is the terminal velocity of a single sphere and its value is set to 1 in our case. In the Tables

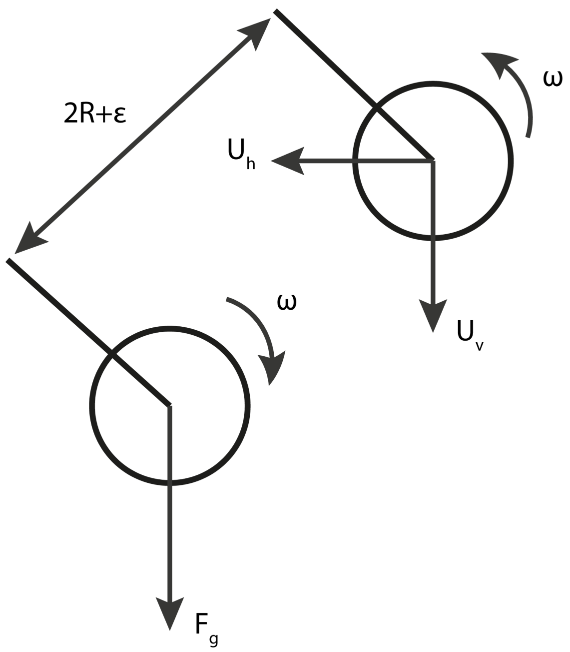

Figure 5.7: The benchmark problem.

5.2 and 5.3 the first three column are *Direct Velocity, Direct Traction and Indirect Velocity Boundary Integral Element* methods of the reference [40]. The present values are provided in the fourth column. The number of elements used in the present computation is slightly different than that of the benchmark case. In the present work spheres with 102 and 401 elements are used. Time step is set to 0.005. The trajectories of the spheres until 2.5 can be seen in the Figure 5.8. The "+" signs represent the positions of the centroids of the spheres at time levels 0.5, 1, 1.5, 2 and 2.5.

For another case the same spheres are left for free fall starting from the rest and $2.5R$ apart from each other. Here the NE for each sphere is 401 and the time step is again $\Delta t = 0.005$. The computed final location and the traction vectors of the spheres with initial positions are shown in the Figure 5.9. As the time evolves, the distance between the spheres are not changed significantly. The time variation of the sphere free fall

Table 5.2: The comparison of solutions for U_v/U_t in the benchmark problem.

NE [40]	DVBIE [40]	DTBIE [40]	IVBIE [40]	**Present**	Analytic
108	1.4651	1.4630	1.4652	**1.4787**	
432	1.4641	1.4642	1.4645	**1.4761**	1.4640

Table 5.3: The comparison of solutions for U_h/U_t in the benchmark problem.

NE [40]	DVBIE [40]	DTBIE [40]	IVBIE [40]	**Present**	Analytic
108	0.07232	0.07956	0.07423	**0.07020**	
432	0.07219	0.07240	0.07250	**0.07099**	0.07233

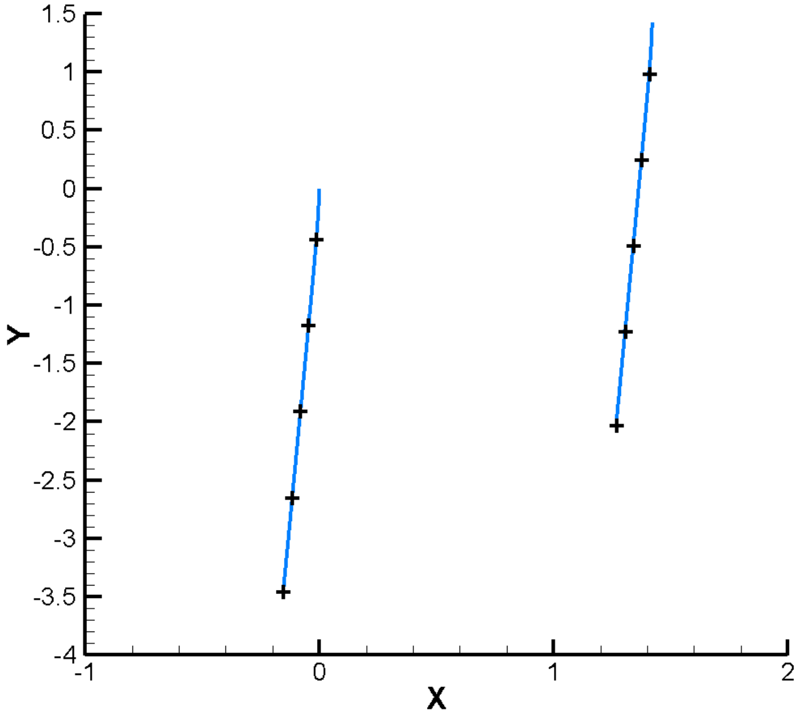

Figure 5.8: The trajectories of the spheres after $t = 2.5$ in benchmark problem.

velocity is shown in the Figure 5.10 and the sphere reaches the terminal velocity higher than that of the single case.

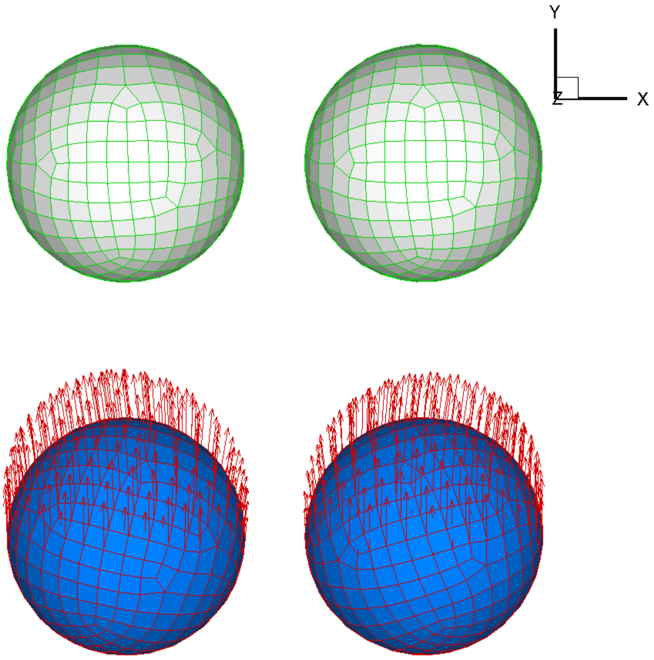

Figure 5.9: The computed locations of the spheres at $t = 2$.

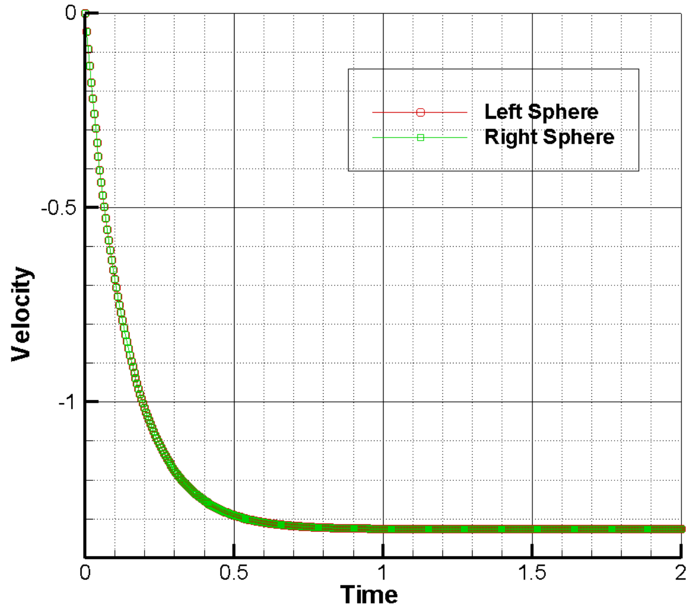

Figure 5.10: The time variation of the fall velocity for two spheres in an unbounded domain.

5.3.3 Three spheres in free fall

As a final case, three spheres are left to free fall that are initially at rest as seen in the Figure 5.11. This time the radius of the spheres are $R = 0.5$. The initial positions of the centres of the spheres are $(0,0,0)$, $(-2,0,0)$ and $(2,0,0)$. Spheres with an element number of 102 are employed and time step is set to 0.005. It is seen that the sphere in the middle falls faster and the other two get closer to each other. And after some time sphere 2 and 3 overlap. Before they overlap, the trajectories of the centroids of the three spheres can be seen in the Figure 5.12. The grey dots on the lines in the Figure 5.12(a) represent the locations of the centroids of the spheres at $t = 10$, $t = 20$ and $t = 30$. The dashed lines in the Figure 5.12(b) represents the centroids of the spheres and solid lines are for point-particles. The present result is very close to the solution in the reference [41].

It is known from earlier works in [42], [43] and [44] that when two particle get close to each other in viscous flow, the effect of the lubrication forces become important. In order to capture these forces with enough resolution close to the contact regions very fine mesh is required.

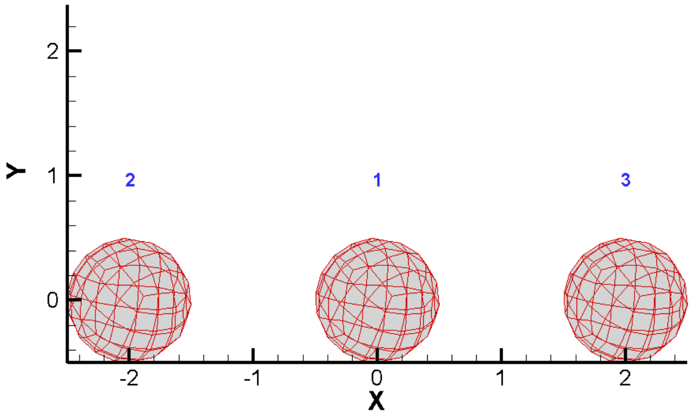

Figure 5.11: Three spheres in free fall.

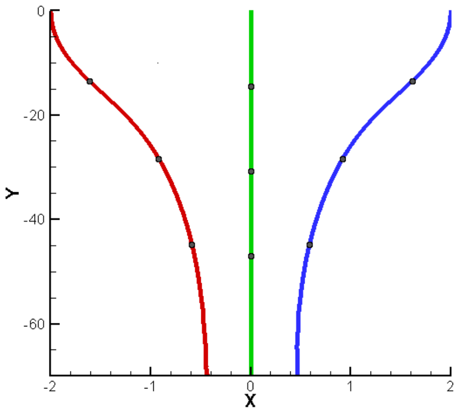

(a) Present work.

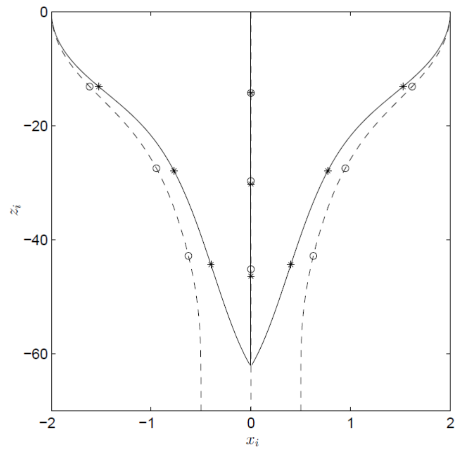

(b) Work of Ekiel et al.

Figure 5.12: The trajectories of the centroids of the three spheres in free fall of present work (a) and the work of Ekiel et al. (b).

6. CONCLUSIONS AND RECOMMENDATIONS

An integral equation method has been developed to solve the three-dimensional Stokes flow. First, the boundary integral equation is constructed using the fundamental solution of the Stokes flow, Stokeslets. After discretization of these equations, the numerical integration is evaluated using the Gauss-Legendre quadratures for non-singular and $tanh - sinh$ quadrature method for singular integrals over quadrilateral elements. In order to avoid the irregularities in the numerical solution, the surface elements are approximated by constructing bi-cubic continuous Hermite polynomial surfaces. The numerical algorithm is initially validated for the three-dimensional unbounded Stokes flow around a sphere. Then the algorithm is applied to the sedimentation of spherical particles. The numerical results indicate that the numerical method is sufficiently accurate for the Stokes flow problems.

REFERENCES

[1] **Youngren, G.K. and Acrivos, A.** (1975). Stokes flow past a particle of arbitrary shape: a numerical method of solution, *J. Fluid Mech.*, ***69***, 377–403.

[2] **Youngren, G.K. and Acrivos, A.** (1976). On the shape of a gas bubble in a viscous extensional flow, *J. Fluid Mech.*, ***76***, 433–442.

[3] **Brady, J.F., Phillips, R.J., Lester, J.C. and Bossis, G.** (1988). Dynamic simulation of hydrodynamically interacting suspensions, *J. Fluid Mech.*, ***195***, 257–280.

[4] **Larson, R.E. and Higdon, J.J.L.** (1986). Microscopic flow near the surface of two-dimensional porous media. Part 1. Axial flow, *J. Fluid Mech.*, ***166***, 449–472.

[5] **Pozrikidis, C.** (1990). The axisymmetric deformation of a red blood cell in a uniaxial straining Stokes flow, *J. Fluid Mech.*, ***266***, 231–254.

[6] **Hancock, G.J.** (1953). The self-propulsion of microscopic organisms through liquids, *Proc. Roy. Soc. A*, ***217***, 96–121.

[7] **Muldowney, G.P. and Higdon, J.J.L.** (1995). A spectral boundary element approach to three-dimensional Stokes flow, *J . Fluid Mech.*, ***298***, 167–192.

[8] **Chan, C.Y., Beris, A.N. and Advani, S.G.** (1992). Second-order boundary element method calculations of hydrodynamic interactions between particles in close proximity, *Int. J. Numer. Meth. Fluids*, ***14***, 1063–1086.

[9] **Duffy, M.G.** (1982). Quadrature over a pyramid or cube of integrands with a singularity at a vertex, *SIAM J. Numer. Anal.*, ***19***, 1260–1262.

[10] **Mousavi, S.E. and Sukumar, N.** (2010). Generalized Duffy transformation for integrating vertex singularities, *Comput. Mech.*, ***45***, 127–140.

[11] **Cortez, R.** (2001). The method of regularized Stokeslets, *SIAM J. Numer. Anal.*, ***23***, 1204–1225.

[12] **Takahasi, H. and Mori, M.** (1974). Double exponential formulas for numerical integration, *Publ. RIMS*, ***9***, 721–741.

[13] **Demidov, A.S.** (2001). *Generalized functions in mathematical physics*, Noca Science Publishers.

[14] **Katsikadelis, J.T.** (2002). *Boundary elements theory and applications*, Elsevier.

[15] **Pozrikidis, C.** (1992). *Boundary integral and singularity methods for linearized viscous flow*, Cambridge University Press.

[16] **Marin, O.** (2012). Boundary integral methods for Stokes flow: Quadrature techniques and fast Ewald methods, *Ph.D. thesis*, KTH Engineering School, Stocholm.

[17] **Cortez, R.**, **Fauci, L. and Medovikov, A.** (2005). The method of regularized Stokeslets in three dimensions: Analysis, validation, and application to helical swimming, *Phys. Fluids*, ***17***, 031504–14.

[18] **Stakgold, I.** (1987). *Boundary value problems of mathematical physics*, SIAM.

[19] **Cunha, F.R.**, **Sousa, A.J.D. and Loewnberg, M.** (2003). A mathematical formulation of the boundary integral equation for a compressible Stokes flow, *Comp. and App. Math.*, ***22***, 53–73.

[20] **Happel, J. and Brenner, H.** (1965). *Low Reynolds number hydrodynamics*, Prentice Hall.

[21] **Hasimoto, H.** (1996). Lorentz's theorem on the Stokes equation, *J. Eng. Math.*, ***30***, 215–224.

[22] **Odqvist, F.K.G.** (1930). Über die randwertaufgaben der hydrodynamik zäher flüssigkeiten, *Math. Z.*, ***32***, 329–375.

[23] **Atkinson, K.E.** (1997). *The numerical solution of integral equations of the second kind*, Cambridge University Press.

[24] **Kim, S. and Karilla, S.J.** (2005). *Microhydrodynamics principles and selected applications*, Dover Publications.

[25] **Ladyzhenskaya, O.A.** (1969). *The mathematical theory of viscous incompressible flow*, Gordon and Breach.

[26] **Tsai, C.C.**, **Young, D.L.**, **Lo, D.C. and Wong, T.K.** (2006). Method of fundamental solutions for three-dimensional Stokes flow in exterior field, *J. Eng. Mech.*, ***132***, 317–326.

[27] **Saxena, A.** (2005). *Computer aided engineering design*, Springer.

[28] **Lee, E.H. and Forsythe, G.E.** (1973). Variational study of nonlinear spline curves, *SIAM Review*, ***15***, 120–133.

[29] **Ferguson, J.C.** (1964). Multivariable curve interpolation, *Journal ACM*, ***11***, 221–228.

[30] **Max, N.** (1999). Weights for computing vertex normals from facet normals, *J. Graph. Tools*, ***4***, 1–6.

[31] **Jin, S.**, **Lewis, R.R. and West, D.** (2005). A comparison of algorithms for vertex normal computation, *Visual Comput.*, ***21***, 71–82.

[32] **Hildebrand, F.B.** (1987). *Introduction to numerical analysis*, Dover Publications.

[33] **Stroud, A.H.** (1966). *Gaussian quadrature formulas*, Prentice Hall.

[34] **Neumaier, A.** (2001). *Introduction to numerical analysis*, Cambridge University Press.

[35] **Atkinson, K.E.** (1989). *An introduction to numerical analysis*, Wiley.

[36] **Borwein, J.**, **Bailey, D. and Girgensohn, R.** (2004). *Experimentation in mathematics*, A K Peters.

[37] **Ye, L.**, (2006). Numerical Quadrature: Theory and Computation, Master's thesis, Dalhousie University, Halifax, Nova Scotia.

[38] **Kundu, P.K. and Cohen, I.M.** (2010). *Fluid Mechanics*, Elsevier.

[39] **Morrison, F.A.** (2013). *An introduction to fluid mechanics*, Cambridge University Press.

[40] **Ingber, M.S. and Mammoli, A.A.** (1999). A comparison of integral formulations for the analysis of low Reynolds number flow, *Eng. Analysis with Boundary Elements*, ***23***, 307–315.

[41] **Ekiel-Jezewska, M.L. and Wajnryb, E.** (2005). Symmetric three-particle motion in Stokes flow: equilibrium for heavy spheres in contrast to "end-of-world" for point forces, **Technical Report**, Institute of Fundamental Technological Research, Polish Academy of Sciences.

[42] **Ishikawa, T.**, **Simmonds, M.P. and Pedley, T.J.** (2006). Hydrodynamic interaction of two swimming model micro-organism, *J. Fluid Mech.*, ***568***, 119–160.

[43] **Zhu, G. and Ingber, M.S.** (2009). Accurate treatment of lubrication forces between rigid spheres in viscous fluids using a traction-corrected boundary element method, *Eng. Anal. Bound. Elem.*, ***33***, 467–473.

[44] **Verdon, N.**, **Lefebcre-Lepot, A.**, **Lobry, L. and Laure, P.** (2010). Contact problems for particles in shear flow, *European J. Comp. Mech.*, ***19***, 513–531.

APPENDICES

APPENDIX A: The Weights and Points for the Gauss-Legendre Quadrature

Table A.1: The weights and points for the Gauss-Legendre quadrature.

	i	Weights	Points
	1	1.0000000000000000	-0.5773502691896257
	2	1.0000000000000000	0.5773502691896257
$n = 3$	1	0.8888888888888888	0.0000000000000000
	2	0.5555555555555556	-0.7745966692414834
	3	0.5555555555555556	0.7745966692414834
$n = 4$	1	0.6521451548625461	-0.3399810435848563
	2	0.6521451548625461	0.3399810435848563
	3	0.3478548451374538	-0.8611363115940526
	4	0.3478548451374538	0.8611363115940526
$n = 5$	1	0.5688888888888889	0.0000000000000000
	2	0.4786286704993665	-0.5384693101056831
	3	0.4786286704993665	0.5384693101056831
	4	0.2369268850561891	-0.9061798459386640
	5	0.2369268850561891	0.9061798459386640
$n = 6$	1	0.3607615730481386	0.6612093864662645
	2	0.3607615730481386	-0.6612093864662645
	3	0.4679139345726910	-0.2386191860831969
	4	0.4679139345726910	0.2386191860831969
	5	0.1713244923791704	-0.9324695142031521
	6	0.1713244923791704	0.9324695142031521
$n = 7$	1	0.4179591836734694	0.0000000000000000
	2	0.3818300505051189	0.4058451513773972
	3	0.3818300505051189	-0.4058451513773972
	4	0.2797053914892766	-0.7415311855993945
	5	0.2797053914892766	0.7415311855993945
	6	0.1294849661688697	-0.9491079123427585
	7	0.1294849661688697	0.9491079123427585
$n = 8$	1	0.3626837833783620	-0.1834346424956498
	2	0.3626837833783620	0.1834346424956498
	3	0.3137066458778873	-0.5255324099163290
	4	0.3137066458778873	0.5255324099163290
	5	0.2223810344533745	-0.7966664774136267
	6	0.2223810344533745	0.7966664774136267
	7	0.1012285362903763	-0.9602898564975363
	8	0.1012285362903763	0.9602898564975363
$n = 9$	1	0.3302393550012598	0.0000000000000000
	2	0.1806481606948574	-0.8360311073266358
	3	0.1806481606948574	0.8360311073266358
	4	0.0812743883615744	-0.9681602395076261

Continued on next page

Table A.1 – continued from previous page

	i	Weights	Points
	5	0.0812743883615744	0.9681602395076261
	6	0.3123470770400029	-0.3242534234038089
	7	0.3123470770400029	0.3242534234038089
	8	0.2606106964029354	-0.6133714327005904
	9	0.2606106964029354	0.6133714327005904
$n = 10$	1	0.2955242247147529	-0.1488743389816312
	2	0.2955242247147529	0.1488743389816312
	3	0.2692667193099963	-0.4333953941292472
	4	0.2692667193099963	0.4333953941292472
	5	0.2190863625159820	-0.6794095682990244
	6	0.2190863625159820	0.6794095682990244
	7	0.1494513491505806	-0.8650633666889845
	8	0.1494513491505806	0.8650633666889845
	9	0.0666713443086881	-0.9739065285171717
	10	0.0666713443086881	0.9739065285171717

APPENDIX B: *tanh-sinh* Quadrature Algorithm.

Initialize: Set $h = 2^{-m}$
For $k = 0$ to 20^m Do:
Set $t = kh$
$x_k = tanh(\pi/2 \cdot sint)$
$w_k = \pi/2 \cdot cosht/cosh^2(\pi/2 \cdot sinht)$
If $|x_k - 1| < \varepsilon$ then exit Do
End Do

Perform quadrature for a function $f(x)$ on $[-1,1]$:
Set $S = 0$ and $h = 1$
For $k = 1$ to m (or until successive values of S are identical to within ε)
Do $h = h/2$
For $i = 0$ to n_k step 2^{m-k} Do If (mod $(i, 2^{m-k+1}) \neq 0$ or $k = 1$) Then If $i = 0$ then $S = S + w_0 f(0)$ Else
$S = S + w_i[f(-x_i) + f(x_i)]$ End If
End If
End Do
End Do
$Result = hS$

Table B.1: The weights and points for *tanh-sinh* quadrature.

	i	Weights	Points
$m = 1$	1	0.78539552480610131	0.0000000000000000
	2	0.48298666707856969	0.67427149224843586
	3	0.48298666707856969	-0.67427149224843586
	4	0.11501081087050929	0.95136796407274693
	5	0.11501081087050929	-0.95136796407274693
	6	9.1715526824894551E-003	0.99751485645722437
	7	9.1715526824894551E-003	-0.99751485645722437
	8	1.3309980971821302E-004	0.99997747719246155
	9	1.3309980971821302E-004	-0.99997747719246155
	10	1.0715566278775086E-007	0.99999998887566488
	11	1.0715566278775086E-007	-0.99999998887566488
$m = 2$	1	0.39269908181303181	0.0000000000000000
	2	0.34740368991293702	0.37720973816403419
	3	0.34740368991293702	-0.37720973816403419
	4	0.24149414492336993	0.67427149224843586
	5	0.241494144923369	-0.67427149224843586

Continued on next page

Table B.1 – continued from previous page

	i	Weights	Points
	6	0.13276956889566041	0.85956905868989664
	7	0.13276956889566041	-0.85956905868989664
	8	5.7505598645436036E-002	0.95136796407274693
	9	5.7505598645436036E-002	-0.95136796407274693
	10	1.9096435898266720E-002	0.98704056050737687
	11	1.9096435898266720E-002	-0.98704056050737687
	12	4.5857917488167982E-003	0.99751485645722437
	13	4.5857917488167982E-003	-0.99751485645722437
	14	7.2562943718654607E-004	0.99968826402835320
	15	7.2562943718654607E-004	-0.99968826402835320
	16	6.6550128457550713E-005	0.99997747719246155
	17	6.6550128457550713E-005	-0.99997747719246155
	18	2.9959253416647420E-006	0.99999920473711468
	19	2.9959253416647420E-006	-0.99999920473711468
	20	5.3578011407953129E-008	0.99999998887566488
	21	5.3578011407953129E-008	-0.99999998887566488
$m = 3$	1	0.19634954087915507	0.0000000000000000
	2	0.19041046485822999	0.19435700332493541
	3	0.19041046485822999	-0.19435700332493541
	4	0.17370184493226357	0.37720973816403419
	5	0.17370184493226357	-0.37720973816403419
	6	0.14918287825378082	0.53914670538796772
	7	0.14918287825378082	-0.53914670538796772
	8	0.12074707244485915	0.67427149224843586
	9	0.12074707244485915	-0.67427149224843586
	10	9.2179731059180328E-002	0.78060743898320040
	11	9.2179731059180328E-002	-0.78060743898320040
	12	6.6384784438579633E-002	0.85956905868989664
	13	6.6384784438579633E-002	-0.85956905868989664
	14	4.5057677315504772E-002	0.91487926326457458
	15	4.5057677315504772E-002	-0.91487926326457458
	16	2.8752799318711383E-002	0.95136796407274693
	17	2.8752799318711383E-002	-0.95136796407274693
	18	1.7177763469252431E-002	0.97396686819567746
	19	1.7177763469252431E-002	-0.97396686819567746
	20	9.5482179478028374E-003	0.98704056050737687
	21	9.5482179478028374E-003	-0.98704056050737687
	22	4.8968756874431234E-003	0.99405550663140219
	23	4.8968756874431234E-003	-0.99405550663140219
	24	2.2928958740888895E-003	0.99751485645722437
	25	2.2928958740888895E-003	-0.99751485645722437
	26	9.6782512840488195E-004	0.99906519645578584
	27	9.6782512840488195E-004	-0.99906519645578584
	28	3.6281471854271566E-004	0.99968826402835320
	29	3.6281471854271566E-004	-0.99968826402835320

Continued on next page

Table B.1 – continued from previous page

	i	Weights	Points
	30	1.1874335055345126E-004	0.99990938469514401
	31	1.1874335055345126E-004	-0.99990938469514401
	32	3.3275064224138556E-005	0.99997747719246155
	33	3.3275064224138556E-005	-0.99997747719246155
	34	7.8103199062781084E-006	0.99999531604122049
	35	7.8103199062781084E-006	-0.99999531604122049
	36	1.4979626706236335E-006	0.99999920473711468
	37	1.4979626706236335E-006	-0.99999920473711468
	38	2.2829150745602266E-007	0.99999989278161239
	39	2.2829150745602266E-007	-0.99999989278161239
	40	2.6789005700243578E-008	0.99999998887566488
	41	2.6789005700243578E-008	-0.99999998887566488
	42	2.3359102839464908E-009	0.99999999914270510
	43	2.3359102839464908E-009	-0.99999999914270510
m=4	1	9.8174770433730948E-002	0.0000000000000000
	2	9.7423334729813779E-002	9.7923885287832330E-002
	3	9.7423334729813779E-002	-9.7923885287832330E-002
	4	9.5205232423445252E-002	0.19435700332493541
	5	9.5205232423445252E-002	-0.19435700332493541
	6	9.1625901678256599E-002	0.28787993274271589
	7	9.1625901678256599E-002	-0.28787993274271589
	8	8.6850922460959559E-002	0.37720973816403419
	9	8.6850922460959559E-002	-0.37720973816403419
	10	8.1092234409036359E-002	0.46125354393958568
	11	8.1092234409036359E-002	-0.46125354393958568
	12	7.4591439122448269E-002	0.53914670538796772
	13	7.4591439122448269E-002	-0.53914670538796772
	14	6.7602186599361083E-002	0.61027365750063889
	15	6.7602186599361083E-002	-0.61027365750063889
	16	6.0373536218834151E-002	0.67427149224843586
	17	6.0373536218834151E-002	-0.67427149224843586
	18	5.3135803533436901E-002	0.73101803479256156
	19	5.3135803533436901E-002	-0.73101803479256156
	20	4.6089865526845374E-002	0.78060743898320040
	21	4.6089865526845374E-002	-0.78060743898320040
	22	3.9400320951428473E-002	0.82331700550640230
	23	3.9400320951428473E-002	-0.82331700550640230
	24	3.3192392217313113E-002	0.85956905868989664
	25	3.3192392217313113E-002	-0.85956905868989664
	26	2.7552077269655934E-002	0.88989140278426015
	27	2.7552077269655934E-002	-0.88989140278426015
	28	2.2528838656410730E-002	0.91487926326457458
	29	2.2528838656410730E-002	-0.91487926326457458
	30	1.8140042458700576E-002	0.93516085752198463
	31	1.8140042458700576E-002	-0.93516085752198463

Continued on next page

Table B.1 – continued from previous page

i	Weights	Points
32	1.4376399658499536E-002	0.95136796407274693
33	1.4376399658499536E-002	-0.95136796407274693
34	1.1207775757953673E-002	0.96411216422354729
35	1.1207775757953673E-002	-0.96411216422354729
36	8.5888817341147217E-003	0.97396686819567746
37	8.5888817341147217E-003	-0.97396686819567746
38	6.4645096395542188E-003	0.98145482667733519
39	6.4645096395542188E-003	-0.98145482667733519
40	4.7741089736171062E-003	0.98704056050737687
41	4.7741089736171062E-003	-0.98704056050737687
42	3.4556052342085801E-003	0.99112699244169877
43	3.4556052342085801E-003	-0.99112699244169877
44	2.4484378435757500E-003	0.99405550663140219
45	2.4484378435757500E-003	-0.99405550663140219
46	1.6958443760133261E-003	0.99610866543750853
47	1.6958443760133261E-003	-0.99610866543750853
48	1.1464479369761704E-003	0.99751485645722437
49	1.1464479369761704E-003	-0.99751485645722437
50	7.5522147501698954E-004	0.99845420876769775
51	7.5522147501698954E-004	-0.99845420876769775
52	4.8391256417362256E-004	0.99906519645578584
53	4.8391256417362256E-004	-0.99906519645578584
54	3.0101863402327747E-004	0.99945143443527462
55	3.0101863402327747E-004	-0.99945143443527462
56	1.8140735926055449E-004	0.99968826402835320
57	1.8140735926055449E-004	-0.99968826402835320
58	1.0567962489365672E-004	0.99982882207287493
59	1.0567962489365672E-004	-0.99982882207287493
60	5.9371675273189875E-005	0.99990938469514401
61	5.9371675273189875E-005	-0.99990938469514401
62	3.2087114007201825E-005	0.99995387100562794
63	3.2087114007201825E-005	-0.99995387100562794
64	1.6637532111078466E-005	0.99997747719246155
65	1.6637532111078466E-005	-0.99997747719246155
66	8.2532713292670465E-006	0.99998948201481852
67	8.2532713292670465E-006	-0.99998948201481852
68	3.9051599529064903E-006	0.99999531604122049
69	3.9051599529064903E-006	-0.99999531604122049
70	1.7568852706582138E-006	0.99999801714059544
71	1.7568852706582138E-006	-0.99999801714059544
72	7.4898133526721274E-007	0.99999920473711468
73	7.4898133526721274E-007	-0.99999920473711468
74	3.0148238773163752E-007	0.99999969889415263
75	3.0148238773163752E-007	-0.99999969889415263
76	1.1414575372121361E-007	0.99999989278161239

Continued on next page

Table B.1 – continued from previous page

i	Weights	Points
77	1.1414575372121361E-007	-0.99999989278161239
78	4.0485978776188192E-008	0.99999996423908089
79	4.0485978776188192E-008	-0.99999996423908089
80	1.3394502849324107E-008	0.99999998887566488
81	1.3394502849324107E-008	-0.99999998887566488
82	4.1146990708282639E-009	0.99999999678719909
83	4.1146990708282639E-009	-0.99999999678719909
84	1.1679551419036902E-009	0.99999999914270510
85	1.1679551419036902E-009	-0.99999999914270510
86	3.0475038111709718E-010	0.99999999978973286
87	3.0475038111709718E-010	-0.99999999978973286

CURRICULUM VITAE

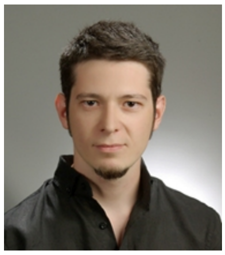

Name Surname: Reşit Kayhan Ata

Place and Date of Birth: Nevşehir 1983

Adress: Uçak-Uzay Bil. Fak. No:310 Maslak

E-Mail: atares@itu.edu.tr

B.Sc.: ITU Astronautical Engineering

Professional Experience:
2011-present: Research Assistant at ITU Astronautical Eng.

PUBLICATIONS/PRESENTATIONS ON THE THESIS

- **Ata K.**, Karaca S. and Şahin M., 2013: An integral equation approach for the solution of the Stokes flow with hermite surfaces. *18. National Congress of Mechanics*, August 26-30, 2013 Manisa, Turkey.